# ZERO-$\hat{n}$ GAP DESIGN VIA MODULATION OF HEXAGONAL PHOTONIC CRYSTAL LATTICE

ATHESIS SUBMITTED TO
THE GRADUATE SCHOOL OF NATURAL AND APPLIED SCIENCES
OF
THE MIDDLE EAST TECHNICAL UNIVERSITY

BY

SHAHRAM MORADI

IN PARTIAL FULFILLMENT OF THE REQUIREMENTS
FOR
THE DEGREE OFMASTER OF SCIENCE
IN
MICRO AND NANO TECHNOLOGY

FEBURARY2017

**ZERO-$\hat{n}$ GAP DESIGN VIA MODULATION OF HEXAGONAL PHOTONIC CRYSTAL LATTICE**

Submitted by **SHAHRAM MORADI** in partial fulfillment of the requirements for the degree of **Master of Sciencein Micro and Nano Technology Department, Middle East Technical University** by,

,

Prof. Dr. GÜLBİN DURAL ÜNVER
Director, Graduate School of**Natural and Applied Science**  _____

Assoc. Prof. Dr.BURCU AKATA KURÇ
Head of Department in **Micro and Nano Technology**  _____

Asst. Dr. SERDAR KOCAMAN
Supervisor, **Electrical Enginering Dept., METU**  _____

Asst. Prof. Dr. EMRE YÜCE
Co-Supervisor, **Physic Dept., METU**  _____


 **Examining CommitteeMembers:**

Prof. Dr. HAMZA KURT
Electrical Engineering,TOBB  _____

Asst. Prof. Dr. SERDAR KOCAMAN
Electrical Engineering, METU  _____

Asst. Prof. Dr. EMRE YÜCE
Physics, METU  _____

Asst. Prof. Dr. SELÇUK YERCI
Micro and Nano Technology, METU  _____

Asst. Prof. Dr. FATIH KOÇER
Electrical Engineering,METU  _____


**Date:**03.02.2017

**I declare that all documents in the following thesis are gathered according to the academic rules including ethical conduct. Moreover, I provided all required references once I used any concept from any paper or thesis.**

Name,Last name:  ShahramMoradi

Signature        :  _____

**ABSTRACT**


**ZERO-$\tilde{n}$ GAP DESIGN VIA MODULATION OF HEXAGONAL PHOTONIC CRYSTAL LATTICE**


MORADI, SHAHRAM

M.Sc., Department of MICRO ANDNANO TECHNOLOGY

Supervisor: Assist. Prof. Dr. SERDAR KOCAMAN

Co-supervisor: Assist. Prof. Dr. EMRE YUCE


February 2017, 93 pages


We study the effect of disorder in the lattice on a photonic band diagram and apply it to form a superlattice in order to examine negative refractive index and finally obtain zero-ñ gap. In addition, the novelty of suggested modulated PhC introduces new ways of controlling light through the complicated lattices. The aim of this approach is to have a deep understanding of dispersion characteristics dependence on the lattice structure by comparing modified structures with conventional lattice types. We design a disordered modulated hexagonal lattice in which the positions of holes vary in the orthogonal direction of applied light direction and study its influence on both effective refractive index and photonic band structure through numerical simulations. The results of this approach are promising enough to utilize them in various applications of on-chip integrated circuits. We applied this class of suggested structure in one particular superlattice to gain zero-ñ gap for the sake of comparison with the reported structures recently.


Keywords: photonic crystal, zero-$\tilde{n}$gap, negative refractive index

# ÖZ

## ALTIGENSEL FOTONIK ÖRGÜ MODÜLASYONU İLE GENİŞ BANT SIFIR KIRICILIK İNDEKSİ TASARIMI

MORADI, SHAHRAM

Yüksek Lisans, Mikro Ve Nano TeknolojiBölümü

Tez Yöneticisi: Asst. Professor Dr. SERDAR KOCAMAN

Ortak Tez Yöneticisi: Asst. Professor Dr. EMRE YUCE

Şubat 2017, 93 sayfa

Fotonik örgü yapılarındaki düzensizliğin fotonik bant diyagramına olan etkisi incelendi ve bu düzensizlik negatif kırılma indisini gözlemlemek ve nihai olarak sıfır kırıcılık indisli bant aralığı elde etmek için fotonik yapıya uygulandı. Ek olarak önerilen yapı ışığın karmaşık örgü yapıları içerisinde kontrolune yeni yollar sunmaktadır. Bu yaklaşımın amacı dağılım özelliklerinin örgü yapıya olan bağlılığını, değiştirilmiş ve olağan yapıları karşılaştırarak derinlemesine anlamaktır. Konumu uygulanan ışığın yönüne dik yönde değişiklik gösteren oyuklar içerecek şekilde düzensizleştirilmiş altıgen örgü yapı tasarlandı ve bu yapının etkin kırılma indisi ile fotonik bant düzenine etkisi nümerik simülasyonlarla incelendi. Bu yaklaşımın sonuçları bu yapıların çeşitli çip üzeri tümleşik devre uygulamalarında kullanılabilmesine olanak sağlayacak kadar umut vericidir. Önerilen türdeki yapı belirli bir süper örgüye literatürdeki yapılarla karşılaştırmak amacıyla sıfır kırıcılık indisli bant aralığı elde etmek için uygulandı.


Anahtar Sözcükler:Fotonık örgü, Bant Sıfır kırıcılık indisi,negatifkırılmaindisi

To My Family

# ACKNOWLEDGMENTS

First of all I would like to thank of gratitude to my supervisor Dr. SerdarKocaman. Besides, I would also like to thank all of the colleagues from METU. Second, I would also like to say my deepest thanks to my parents and wife who helped me a lot in finalising my M.Sc. thesis.

# TABLE OF CONTENTS

x

# LIST OF TABLES

**TABLES:**

# LIST OF FIGURES

**FIGURES:**

# LIST OF ABBREVIATIONS

PBG.................................................... Photonic Band Gaps

FDTD.................................................. Fnite-Difference Time-Domain

PhC.................................................... Photonic Crystal

MPB................................................... MIT Photonic Bands

PIC..................................................... Photonic Integrated Circuit

NIMs.................................................. Negative Index Materials

PhCs................................................... Photonic Crystals

GMRs................................................. Guided Mode Resonances

UV..................................................... Ultra Violet

DUV................................................... Deep Ultra Violet

KrF.................................................... Kind of excimer

ArF.................................................... Kind of excimer

HC-PCF.............................................. Hollow-Core Photonic Crystal Fiber

SW..................................................... Surface Wave

WGMs................................................ Whispring Gallery Modes

TIR.................................................... Total Internal Reflection

Q-factor.............................................. Quality factor

PL...................................................... Photoluminescence

DBR................................................... Distributed Bragg Reflection

DFB..................................................... Distributed Feedback

ROW.................................................... Resonant-Optical-Waveguide

EFCs.................................................... Equi-Frequency Contours

PPC..................................................... Plasma Photonic Crystal

# CHAPTER 1

# 1 INTRODUCTION

## 1.1 Overview

It is now well recognized that photonic science and the related technologies have been playing an essential role in the rapid progressing and development of today's information and communication technology. However, by considering huge demand of data communication in $21^{st}$ century, the sole option of using electronics is changing and photonic integrated circuits (PICs) with which the speed of data transfer reached to the terahertz scale. A PIC is a device that combines various components similar to an electronic integrated circuit which functions on optical wavelength such as the visible or near infrared range. Integration of various optically active and inactive devices operates on one single chip made the developments in this field especially exciting. In this chapter, we go over the general concepts and applications of the developing branches of photonic science and also discuss some of the typical devices that will help understand what we study at this thesis clearly.

## 1.2 Devices in the photonic field of science

### 1.2.1 Quantum Dots

As discussed above, photonics has the potential of enabling high-speed and wide bandwidth data handling beyond the limitations of electronics technologies. One of the major subareas here is about the studies on quantum dots. Light-matter interaction as an outlet of achieving high-speed communication and information is considered as a key factor in this field. By reviewing all developed nanophotonic devices, the idea of light-matter interactions can be summarized by confining light inside a small-engineered geometry [1]. This means that light with small mode volumes has the capability of being

manipulated for optical information processing at low level of energies which could be as low as a single photon level. Promising efforts in this field that develops and give rise to coherent control of light through strongly coupled nanophotonicdevices such quantum dots and PhC cavities constitute the main interest. As quantum dots are made of particular semiconductor "artificial atoms" that can act as efficient photon emitters, they behave as stable quantum memories. After embedding them in a PhC cavity [3] that spatially confines light to sub-wavelength one can attain the desired strong coupling regime. In strong coupling regime, these interactions are large enough that even a single photon can obtain the ability of creating a fabulous nonlinear response in an atomic system. Such single-photon nonlinear capabilities are highly desirable for quantum information processing [2] where atoms serve as quantum memory elements and photons act as required carriers of quantum information. This kind of device platforms provides a roadway towards compact integrated quantum on-chip networks that could serve as fundamental components in building quantum computers. Researchers study and demonstrate a quantum transistor, where a single spin in a quantum dot under particular conditions switches the state of a photon [4]. It is also well studied the coherently control of atom-photon interactions on picoseconds timescales based on tailored quantum states of light in a certain cavity [5]. As a conclusion, this technology grows in a way where quantum dots embedded in PhCs based devices will be crucial for the development of chip integrated quantum systems that has could be a real tuning point photonics science.

### 1.2.2   NanoOptomechanical Devices

Optically tuned physical movement, which are compatible for on-chip integration, have been made possible by opto-mechanical effects [6]. As an example, many devices such as sensors [7] gratings, [8-9], ring resonators [10-11] and movable mirrors [12-15] need tunable lasers and optomechanical elements can help for desired longitudinal mode of introduced pulse through the cavity and controlling the line width of the laser transition. Another applications of these devices can be explained through optical actuation that

relies on optical forces allowing PICs elements to be controlled by light force, and this is based on nonlinearity of optical field [16-18]. Some experiments demonstrate such nonlinear behavior in aa microwave regime metamaterial structures [17]. This approach was extended to the regime using a dielectric material and its optomechanical metamaterial properties. An all-dielectric metamaterial has been shown to possess an optomechanical nonlinear property that gives rise to modulation of light with light at megahertz (MHz) range of frequency [19]. Moreover, nanoscale positioning is obtainable, since optical gradient force is exerted on the free-standing waveguide while light flow is evanescently coupled to either a nearby waveguide or a dielectric substrate [20-21]. This leads to changing effective refractive index of the free standing waveguide with the nanoscale position [22-24]. However, the amplitude of the optical gradient force is proportional to the gradient of the electromagnetic field and this field is significantly enhanced by proper components such as PhC cavities and ring resonators with high quality factors [23-24]. As a result, on-chip applications of optomechanical force started to develop and realize the aim of both sending and receiving mechanical signals among a variety of platforms and design capabilities that come with PhCs play a key role in this development.

### 1.2.3 Plasma photonic

Photonic Band Gap (PBG) as an essential parameters of photonic science needs to be controlled since the complicated components of a PIC progress with vast alternative range of frequencies. To obtain a tunable PBG, the refractive index of a PhCcan be changed through the magnetic permeability of one of the constituent materials used in PhC. Meaning that the dielectric of utilized component in PhC should depend on some external parameters. [25]. Utilization of tunable laser is one of the most important applications of photonic science and usingionized gases, or plasmas, for light radiation in the Ultra Violet(UV) and Deep Ultra Violet (DUV) spectral range needs this tools of controlling PBG as discussed. However, they are still a medium of choice for laser sources at wavelengths that are not achievable by solid-state technology. For example,

KrF and ArF gas mixture plasma based lasing media are included in gas-phase materials that produce traditional excimer gas laser. However, using these typical lasers suffer from having a huge volume and lack of tenability for complicated systems. Plasma-based laser operation miniaturizes its physical package using plasma PhC (PPC) that contains extra components of controlling PBG rather than conventional PhCs. For example, generation of a long and stable plasma column inside the core of argon filled Kagome hollow-core PhC fiber (HC-PCF) is reported [26].These laser generation is based on conversionof NIR pulsed laser with stimulated Raman scattering [27], soliton dynamics [28], or high harmonic generation [29] and they are different from case to case. Therefore, compatibility of PPC for these types of generators is accentuated since their ability of matching in mentioned regime.These works proved that micro-confining usingthe fourth state of matter within photonic structures such as HC-PCF is now possible and in progress. In other words, it opens the way toward a new research topic named "plasma photonics."

### 1.2.4   Micro cavity

By reviewing the history, Whispringgallery modes (WGMs) were suggested by Lord Rayleigh in 1910. Micro-cavities, as one particular WGM structures, take advantages of total internal reflection (TIR)to confine and enhance light energythrougha smooth and curved surfaces [30]. Possible applications of using micro-cavities, can be addressed in integrated micro-optics devices, such as optical filters [31], biological sensors [32-33], light emitting devices [34] and quantum optics light sources [35]. In addition, in advanced level of utilization, variety of micro-cavity structures have been proposed, such as micro-columns [36], micro-rings [37], micro-disks [38], and microtoroids [39]. Wavelength tuning is a challenging issue in utilization of these types of devices, for example in conventional semiconductor micro-cavities because of the intrinsic energy level constituents of semiconductors it was a difficult step to proceed. However, possible solutions like Dye-doped lasers existssince the volume of enhanced energy that they provide in one pulse [30]. On the other hand, the enhanced energy gives rise to losing

single modeoutput spectra, which enormously influence the output.This concerns end up with different methods that inspire researchers to suggest, such as multi layered films or gratings with distributed feedback (DFB) or distributed Bragg reflection (DBR) components [40-41].It is noticeable that the huge gap between proposed conventional optical cavities and micro-cavities is the effects that arise from the miniaturized dimensions of the structure. In other words, this level of designing and fabricating provide a useful chance of observing Quantum effects of the light's electromagnetic field like spontaneous emission rate and even behavior of atoms [42].

### 1.2.5 Photonic crystal

Among all those selected devices that we want to skim briefly the role of PhCsare more accentuated rather than the other components of photonic integrated circuits (PIC). However, it is undeniable that photonics is not independent of electronic integrated circuits (ICs) and many of the date processing processes still with electronic chips. This limitation is originated from basic characteristic of light in an offered media. Unlike the electrons in media, the confining of light or even storing it in a small volume is a hardship job. In addition, controlling the speed of light is even another issue which is correlated to the weak interaction of light with matter.PhCs are expected to obviate all those requirements to form a satisfying tools of operation.This thesis reviews what a PhC is and what it can do, particularly for photonics technologies and describes how effective is an engineered structure. Comparing dispersion, variation of refractive index for each frequency inside the same material,influenceonPhCs which give rise to the various light emissionresults such as self-collimated beam emission [43-44], negative refractive index materials [45-46], and zero-ñ gap effects [47] opens huge possibilities to solve all above mentioned problems. Meaning that, they could bring new methods to manipulate the light flow in PhCs like what we are expecting in ICs. The light emission directionin one PhC is determined by group velocity current of lightin the mentioned PhC,$v_g = \nabla k\omega(k)$.Therefore, the Equi-Frequency Contours (EFCs), plays major role in determination and expectation of light flow since in the Bloch modes that forms by cross

sections of the computed dispersion values in surface of momentum space are determining the propagation direction and characterizing the flowing of lights in PhCs and to design the desired dispersion based PhC.For example, optical devices that we described previouslyand even others that we do not explain such asnanochannel waveguides [48-49], beam splitters [50], super lenses [51], de-multiplexers [51] and so on can be included as an achievements of mentioned approach.The analysis of optical components with desired optical featuresdevelops since advances in fabrication procedure with sub-wavelength size scale are in a rapid growth. In other words, these attempts have ended up with the rapid growth of(PhCs) field of study, providing usefulchances for having progressed new device periods for a vast range of applications. A PhC is, by definition, an artificially engineered structure whose refractive index (n) is modulated with a particular periodicity comparable to the wavelength of light in the utilized material [52]. Moreover, they enable various novel ways of manipulating light in proper medias beyond those limitations for existed conventional materials in nature. All attempts s to realize PhCs have focused mostly on planar (2D) structures because of their potentialof well-developing microelectronic chip fabrication methods, possibility of combining in oneunified planar (2D) platform on top of a substrate, and their close relation to the previousgeneration of integrated optic circuits [53]. However, existence of photonic band gaps also creates strong light confinement that gives possibility of reducing energy consumption of optical devices.existence of photonic band gap at higher dimensions (3D) reported last decades [54-56]. There are applications such as beam forming and dispersion controller in which all dimensional structures using threedimensions (3D) PhCs are highly proceededcases to get rid ofany issue of coupling light flow into and out of the designed planar platform of chip. Moreover, recent advances in nanoscale materials and fabrication methodslike self-assembly [57], multi-beam interference lithography [58], and multi-photonslithography [59] have provided the unique chances to fulfillqualified 3D PhCs at anacceptable cost level that can be offered to use as an optical elements in such devices. In a summery, to have complete

6

advantages of photonics over electronics, one must break through the limitations of current photonics by tightly squeezing an applied optical pulse within a miniaturized volume such as cavity and control the speed of light flow dynamically [60]. In chapter three, we study some tools and possibilities of governing light merely by applying governing rules and parameters in this case.

**CHAPTER 2**

**2 THEORY**

In this chapter, we provide the relative concepts, which are necessary to understand them as a fundamental rules of governing what we obtained in the photonic crystal field. It is noticeable that what we obtained are based on numerical computation of governing equations which we address some of them that is well explained in [61] that used numerical methods of examination. Moreover, the results of this thesis is merely simulation which require setting a particular boundary condition on a bounded domain and they can be applied to our modulated PhCs or any other desired geometry. The MIT Photonic-Bands (MPB) [70] and Meep, are a free software packages to program and model electromagnetic system which MPB mainly is used to compute band diagrams and eigenfields for the crystals, however, Meep perform time-domain (FDTD) simulations of any modulated electromagnetic structures with one, two and even threedimensions to calculate transmission spectra, resonant modes and many other related problems. We applied our suggested geometries to simulate modulated disordered PhC and the results will be discussed in the next chapter.

## 2.1 Governing Equations

Remarkable progress has been made over the past decades in the study of nanoscale PhCs and some other metamaterials. The ability to accurately calculate the eigenmodes and band structures of such structures is a critical step to develop these types of devices which mentioned some of them in first chapter. By skimming the path of this progress, one clearly notices that the computation of band structure were focused on frequency-independent dielectric mediums earlier. However, some software packages, MPB and Meep, make us able to calculate photonic band structures of those material systems with frequency-dependent permittivity [62-63].

## 2.2　Computational tools

Finite difference, finite element, boundary element, localized Gaussian-Hermite are all computational methods in the frequency domain to solve equations based on the time-harmonic Maxwell equations. Starting with the Maxwell's equations help one to have a clear understanding of basic process of what we did to obtain results of light propagation through the suggested modulated structure. However, Maxwell's formulas are written in different forms and governing rules of light-matter interaction according what is well explained in [62] will be:

$$\nabla \times E(x,t) = -\frac{1}{c}\frac{\partial B(x,t)}{\partial t} \tag{2.1}$$

$$\nabla \times B(x,t) = \frac{1}{c}\frac{\partial D(x,t)}{\partial t} \tag{2.2}$$

$$\nabla . D(x,) = 0 \tag{2.3}$$

$$\nabla . H(x,t) = 0 \tag{2.4}$$

In which c, E, B, H and D are the speed of light, electric field, magnetic field, magnetic induction, and the electric displacement respectively. Note that all parameters are dependent of time and positioning ,which occurs after interacting of light with matter. The Maxwell's formulas can be re-written in the constitutive equations form to solve above mentioned relations in a particular given boundary conditions based on what a designer applied in terms of material properties and geometries. Thus, the constitutive equations based on material property can be:

$$D(x,t) = \varepsilon(x)E(x,t) \tag{2.5}$$

$$B(x,t) = H(x,t) \tag{2.6}$$

By considering non-magnetic material the dielectric profile $\varepsilon(x)$ is a position-dependent permittivity that represents solutions of Maxwell's equation in any points according to the medium's property.Since our geometry has periodicity, then the mentioned dielectric profile, which represents optical characteristics of our structure, shows the lattice periodicity in this form:

$$\varepsilon(x + X) = \varepsilon(x) \tag{2.7}$$

To sum up all periodic profiles through the given lattice by Fourier transform, one can simply integrate all acceptable (x) including their translations X to form a plane wave depending on wave vectors. To analyze above mentioned equation in whole we can write it in this form:

$$\varepsilon(x) = \int g(r)e^{(ir.x)}\, dr \tag{2.8}$$

In which g(r) is defined as the coefficient on the plane wave with the wave vector (r).

$$\varepsilon(x + X) = \int g(r)e^{(ir.x)}e^{(ir.X)}dr = \int g(r)e^{(ir.x)}dr \tag{2.9}$$

To show periodicity of dielectric dependent on position, $\varepsilon(x)$, Fourier transform g(r) can be given with an exponential term,$e^{(ir.X)}$, in which the g(r) is either 0 or $l$. We can extract those values that have 1 since the Fourier transform asigns zero value everywhere except for the values of (r) that $e^{(ir.X)} = l$ for all X vectors inside the suggested lattice. Thus, all wave vectors r which have the exponential terms equal to

11

$l$ are acceptable to build a lattice with a periodic dielectric profile in which $(r.X = 2\pi l)$, for all lattice vectors (X) and integer value of $(l)$. The exponential term of dielectric profile, will created vectors (r) that are called reciprocal lattice vectors.We designate by the letter G for the mentioned reciprocal lattice. All included vectors of reciprocal lattice shape a different lattice in new position, that is, the summation of all created new vectors that arranges so many new reciprocal lattice vectors through the suggested lattice.The volume where the reciprocal lattice forms in 2 or 3 dimensions, is called reciprocal space of suggested unit cell.

## 2.3   Brillouin Zone in Hexagonal lattice

It is typical to select the value of T in (k = k'+T) to shrink |k'| down, i. e., to have as near to the adjacent of base of what we assumed as a reciprocal lattice. Meaning that |k'| is necessary to be consideredcloser to the base of reciprocal latticerather than to any other possible cells of suggested reciprocal lattice.In this fashion, Wigner-Seitz cell can be extracted from the given reciprocal lattice. Since the extracted Wigner-Seitz cell cannot be shrieked down more we can call it irreducible Brillouin zone of determined unit cell. In (Figure 2.1) the irreducible Brillouin zone is shown that is labeled and characterized by different wave vectors and the eigenwave is clarified in each suggested wave vectors.
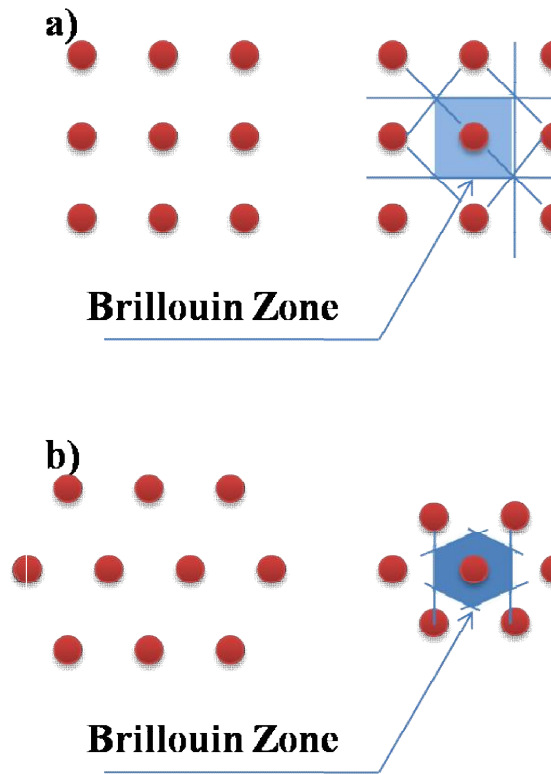
Figure 2.1 - The corresponding first Brillouin zone of a two-dimensional,(a) square lattice and (b) hexagonal lattice  and their Brillouin zone (blue area).

In our thesis, the hexagonal structure is the basic matter of discussion and its irreducible zone is shown in (Figure 2.2. b) in which the two wave vectors characterized the periodicity through the whole hexagonal lattice and the lattice constant is considered as the distance between center of holes in K direction with two vectors that is shown in (Figure 2.2. a) and the radius of each cylinderical holes/rods is considered "r". It is noticeable that the addressed hexagonal structure can be engineered in either high dielectric film like silicon with lower dielectric (holes) or vice versa.
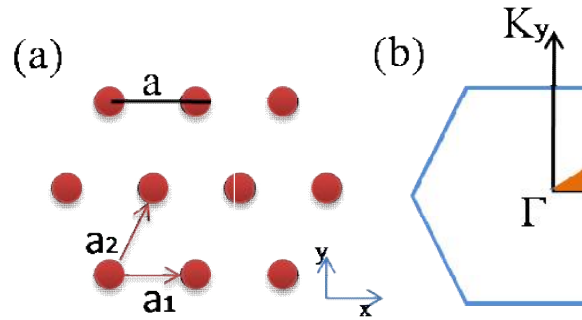
Figure 2.2 - (a) Hexagonal distributionwith lattice constant of "a", (b) irreducible Brillouin zone (orange triangle) starting from the centre, GammaΓ, towards M and K directions.

## 2.4 Hexagonal distribution and superlattice structure

Disordered geometry is one of the inevitable parts of fabrication, particularly in Nanoscale engineering of materials that has been an interesting topic of investigation recently [65-68]. The theory of hexagonal structure for creating a 2D periodic PhC on three dimensional structure is based on a particular triangular holes (cylindrical) in which one of them assumes as a Gamma (the center of axis) and two other holes aligns in K direction, reciprocal lattice directions, with a certain distance which is called lattice constant. In addition, the bisector of created angle between those K-directions makes M direction in the k space (Figure 2.3).
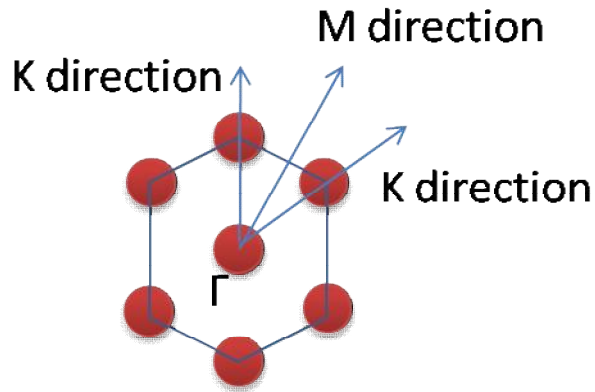
Figure 2.3 - Schematic of hexagonal distribution and its reciprocal lattice directions

As a result, the M and K direction make the $\theta$ angle in regular hexagonal. It assumes 30 degree and K direction lines will make 60 degree with each other due to the symmetric holes in two side of the Gamma. In order to have hexagonal structure, this unit cell should be supposed as a base of two defined directions since the 2D periodic PhC is desired. In order to compute photonic Band Gap (PBG), using MPB, we define one cylindrical hole in Gamma position at (0,0,0) of Cartesian space, then extend the structure in a way that all other cylindrical holes produces through the lattice symmetrically. For the sake of simplicity, creating two vectors of elementary unit cell is so useful and it leads to have iteration of previous vectors constituent and consequently designing of the new created component (Figure 2.4. a).

a)
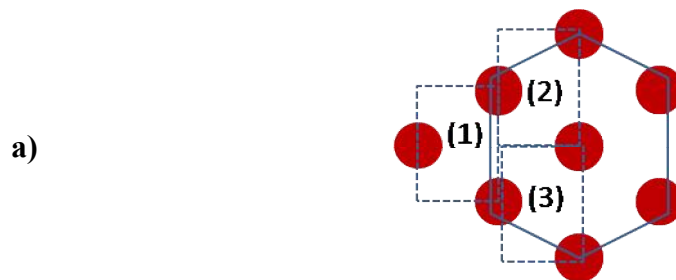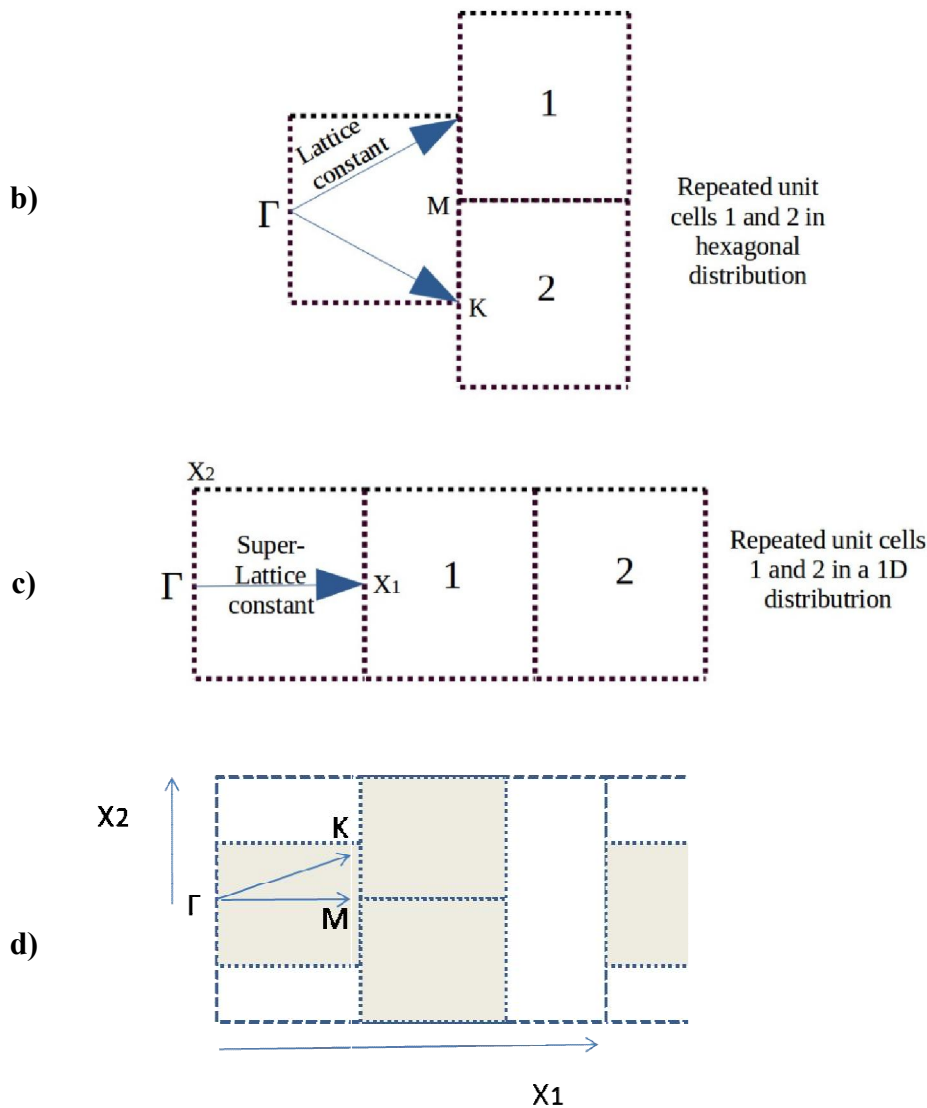
Figure 2.4 - Distribution of cells through the lattice; a) generation of hexagonallattice from iteration of unit cells, b) generation of cells c) generation of superlattice (1D distribution) of generated unit cell, d) schematic of both unit cells inside the generated periodic superlattice

In the (Figure 2.4.b) and (Figure 2.4.a) two different distributions, triangular and 1D, are addressed respectively. For the complicated structures such as combining two class of PhCs to form a superlattice we can also have different periodicity directions with witch the computation of dispersion relation versus the direction in reciprocal space is possible (Figure 2.4.d). For these types of superlattices we expect multiple

16

irreducible Brillouin zone in one direction since in K-space there might be numerous unit cells.

## 2.5 Suggested methods of analysis

### 2.5.1 Analytical method of analysis

Finite-difference time-domain (FDTD) method is one of the strong tools of simulation, as the duration of simulation for computational process is reduced enormously and it depends on the number of the meshed grids in the calculation domain (for example it is in the order of N*N in 2 dimensions). In order to solve Maxwell's equations by extracting one Eigenvalues form out of the equation, the plane wave expansion method (PEW) is a useful technique to solve band structure (dispersion relation) of specific PhC geometries. A Finite Element scheme in a non-orthogonal coordinate system, compute the band structure of one photonic crystal (PhC) including super-lattice. The procedure can easily be applied for any other integrated structure, which can have both the dielectric elements combined with metal components. However, our structure is not metallic type and it is 0.32 [um] thick silicon with engineered cylindrical holes (air) inside the silicon on top of 1 [um] silicon dioxide. Recently, the FDTD method is applied to calculate superlattice photonic band gap, both guided/surface modes. In 2D PhCs, the combination of any periodicity of boundary conditions with a surrounded perfectly matched layer (PML) uses for obtaining of the boundary values. The full-wave analysis is one of the reliable FDTD methods is also suggested for of guided modes in some PhC fibers since it uses real variables of applied components. As a result, the FDTD method can be considered as promising tools for solving Maxwell's equations. It introduces to solve a wide variety of problems related to electromagnetic fields, such as PBG calculation, scattering phenomena's, circuitry elements in electronic, wave propagation ,radiation analysis in antennas, etc. In this thesis, we chose MPB to the

calculation of modal solutions of Maxwell's equations over both inhomogeneous and periodic geometry.

### 2.5.2 Boundary conditions

Two types of boundary conditions with which the constant iteration method of computation is possible are introduced in this thesis. First, physical boundary condition that is determined with the lattice size and dimensions, including properties of designed materials inside a Perfect Matched Layers (PML). Second, numerical boundary condition in which some governing equations assumes to be calculated inside a grids of computation. In order to solve the equation with respect to the limited volume of date, it needs the edge of grids to be determined by numerical boundary conditions. In other words, the calculation process needs some values from outside of the limited grids. We obtained photonic band gap structure with respect to the above mentioned conditions and also the physical boundary conditions as below [71]:

1. Normal components of B and D are continuous across the interface of two different utilized dielectrics in the structure.

2. Tangential component of the wave vector is continuous across an interface of two different dielectrics.

3. Both of the electric and magnetic field normal to the interface are discontinuous across the interfaces.

4. Both of the electric and magnetic tangential components are continuous across the interface.

As a result, all components are continuous except the product of permittivity and permeability changes in the interface based on constitutive relations which dictate the new values of fields after interacting with materials. When calculating the band

structures of PhCs, one normally selects one of the unit cells of the computed lattice in the finite computation domain, and uses the applied periodic boundary condition, which satisfies the Bloch theory of photonic band gap. It is noticeable that constitutive relations express the existence of new sources P and M in terms of the fields E and H, that is $P = f[E]$ and $M = f[H]$ and they are equivalent to $D = f[E]$ and $B = f[H]$ which have linearity in most practical situations of interacting light with matter for PhC applications. As all linear equations are often addresses in terms of the electric and magnetic susceptibilities $\chi_E$ and $\chi_M$ then we can rewrite the secondary sources that are necessary for computational process as below [72]:

$$P(r) = \varepsilon_0 \chi_E(r, \omega) E(r) \, , \, \mathrm{M}(\mathrm{r}) = \chi_M(r, \omega) H(r)$$

Considering that the permeability and permittivity are:

$$\mu = (1 + \chi_E) \, , \varepsilon = (1 + \chi_M)$$

Thus, for what we considered to the boundary conditions one can simply follow the expected rules which mentioned in (Figure 2.5).
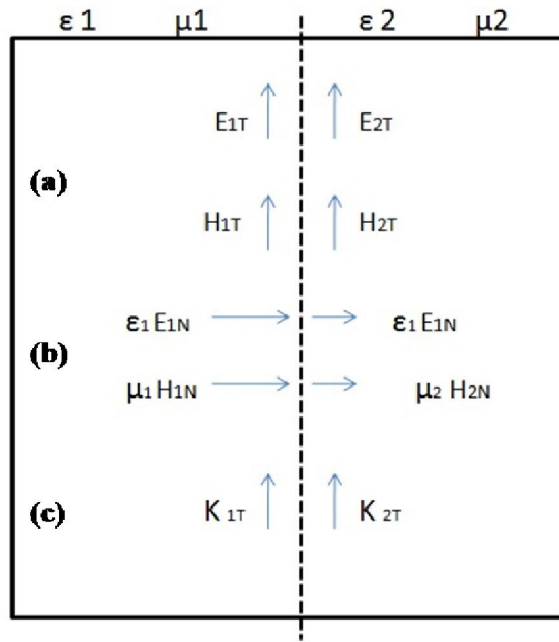
Figure 2.5 - Boundary conditions for an interacted electromagnetic wave in the interface of two different medias, (a) tangential components of H and E fields are considered continuous across an existed interface, (b) fields normal to an existed interface are considered discontinuous across an existed interface (note that normal components of B and D are continuous across an existed interface), (c) tangential component of a wave vector is considered continuous across an interface.

# CHAPTER 3

## 3 MODULATED SOLUTION

In this chapter, our attempts are focused on reviewing previous work of researchers that utilizes the photonic crystals in a novel way; getting a negative refractive index which is not possible in natural materials, and then apply it to obtain a zero average index.In order to cover this intention, we firststart from the simple computation of band diagram of a particular photonic crystal and demonstrate how the negative refraction can be obtained.  Then, we discuss how to obtain zero average index in the following description. To do this, we need a material with a positive refractive index. Since the positive refraction is the natural case, previous studies have used a regular slab waveguide. We discuss how to get positive refractive index from the slab waveguide and then combine the slab waveguide with photonic crystal that has negative refraction that results in a superlattice which is a 1D photonic crystal itself. We then analyze the properties of this superlattice. We also study the transmission spectra for the cases mentioned above.

### 3.1   Photonic band diagram computation of a hexagonal lattice

Here, we study a photonic crystal that is similar to a case in the literature to get negative refraction which use a standard silicon-on-insulator wafer with 0.32 [um] thick silicon on top of 1 [um] silicon dioxide [80]. The parameters (r/a = 0.32, h/a = 0.64) were specifically chosen in order to get negative refraction in the optical communication wavelength.The calculated band diagram is shown in (Fig. 3.1). Previous class of structures, crystal-slab superlattices, to see how effective is each case among suggested methods of combining LIM & PIM to gain zero-ñ gap. Here we study a PhC with a particular parameters to gain a PBG at (a/λ = 0.2875)with a

0.32 [um] thick silicon on top of 1 [um] silicon dioxide that is shown in (Figure 3.1.a.b.).

a)



b)
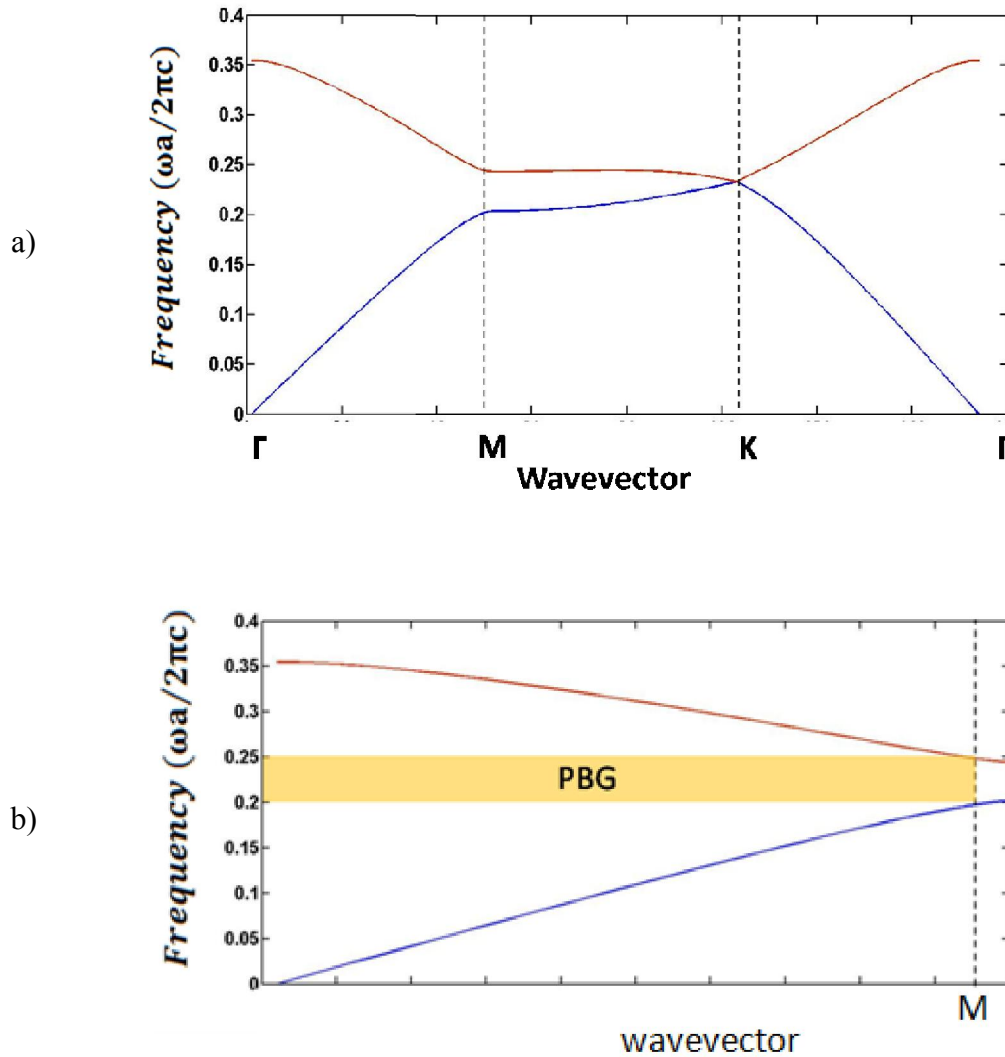


Figure 3.1- PhC band diagram for TM (odd) mode, (a) band diagram; (b) zoomed PBG with an orange colour bar

In the (Figure 3.1), we are focusing on the Γ-M direction and there is a PBG at the angular frequency of 0.585.

22

## 3.2 Negative Vs Positive

Next, we study how a point source propagates across this crystal for a variety of different frequency values. In order to make the take away point clearer, we will use a 2D structure with the similar parameters.
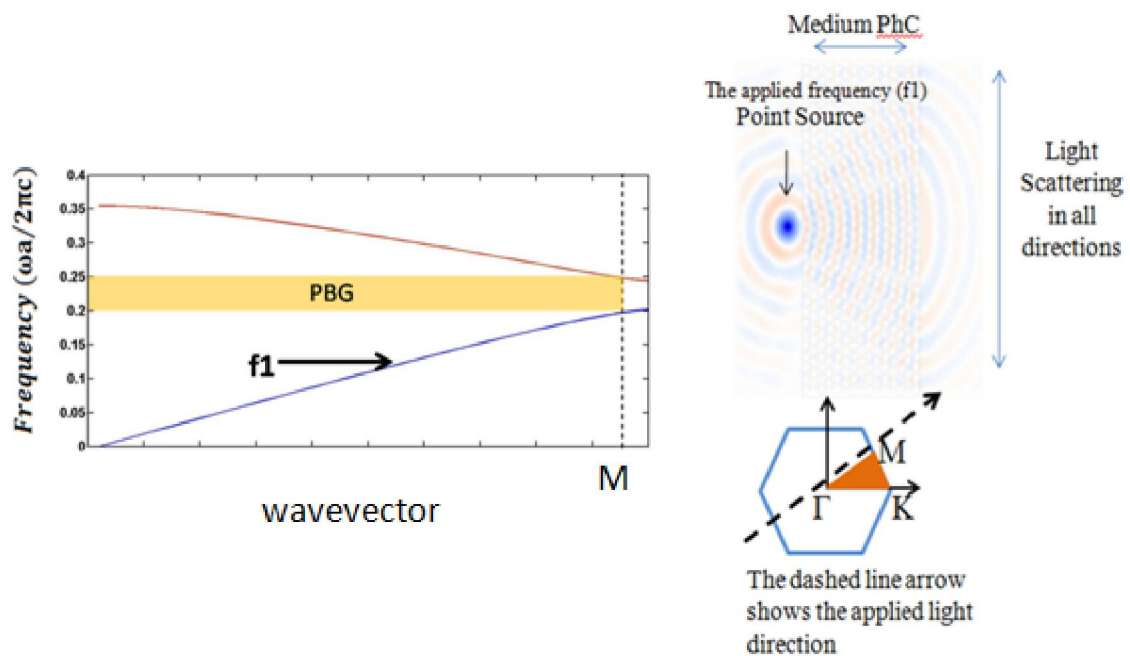


Figure 3.2- Typical light matter interaction in a range of positive refractive index frequencies

In (Figure 3.2), we chose a frequency from the first TM band on the band diagram. As it can be seen from the figure, this section of the photonic band diagram has a positive slope in the Γ-M direction. Then, once the point source is placed in front of the lattice facing the Γ-M direction and the field distribution is calculated, it is seen that the field is diverging, as it is the case for all the natural materials.

In (Figure 3.3), we present the results of our simulations where we repeat the exact same procedure for a frequency from the second TM band. In our thesis, all

computed results are TM (odd) mode but they can be considered in TE (even) mode as well.
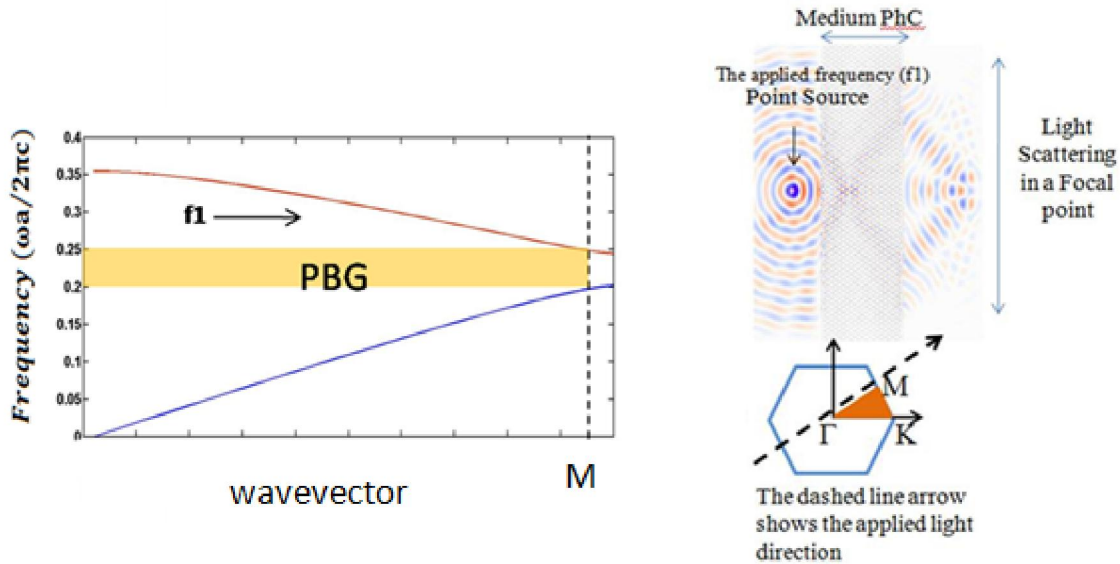


Figure 3.3 - Schematic of light flowing through a 2D PhC with a=0.5 [um], r/a=0.39 cylindrical hole (air) inside the 0.32 [um] on a silicon dioxide substrate with 1 [um] thickness. The isotropic point-source is propagating with normalized frequency of a/λ = 0.306

As it is clear from the band diagram, this time the frequency is chosen from a particular section of the spectrum where the band diagram has a negative slope for the Γ-M direction.When we compare the field distribution with the previous case, there is an unconventional behavior for the second case.

When we analyze the field distributions for the two case, we see an optical path that is represented by the graphics in (Figure 3.4).
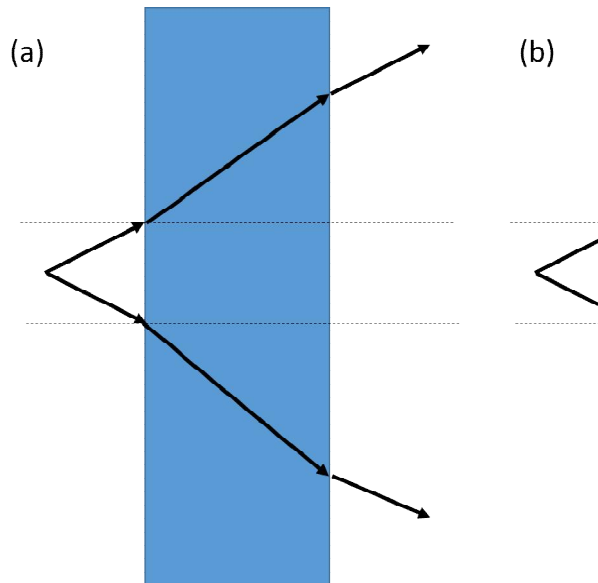
Figure 3.4 - Optical path light rays once the medium has a) positive index b) negative index

In order to be able to explain this behavior, we use the famous Snell's Law which is stated below and it is clear that the optical path in the second case is only possible if the refractive index of the medium is negative.

$$\sin \theta_1 * n_1 = \sin \theta_2 * n_2 \qquad (3.1)$$

This result is actually not surprising as the effective refractive index will be determined by the derivative of the frequency with respect to wavevector and that precisely corresponds to the slope of the band diagram. In addition, this is also why negative refraction results in uperlensing that can defeat diffraction limit and the light is focused even if there is no curvature on the lens [78].

In order to support the result above, we repeat the same calculation with another frequency that also has the negative slope on the band diagram. The simulation results are shown in (Figure 3.5).
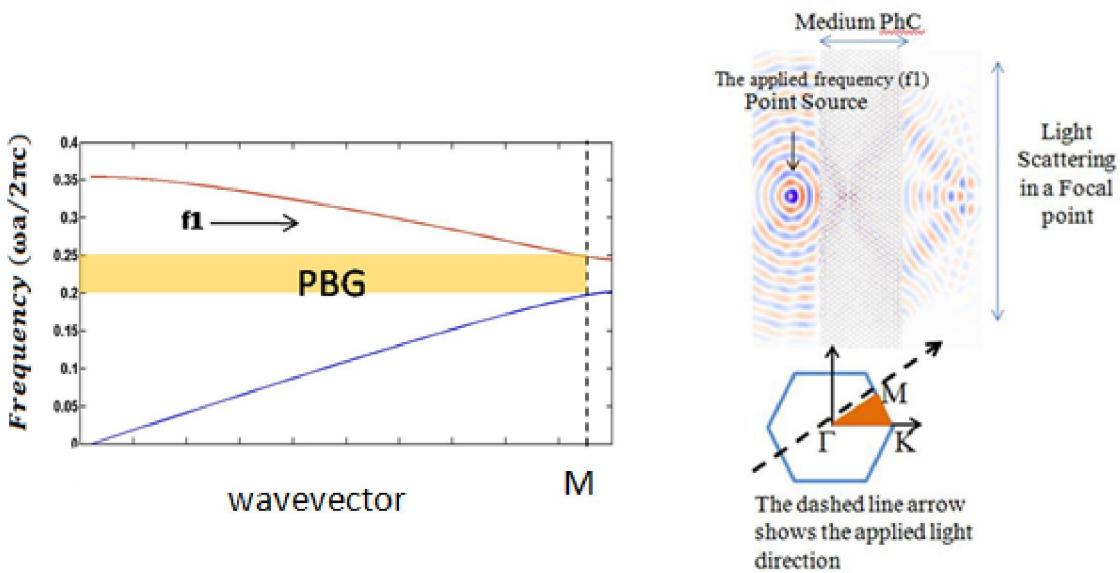
Figure 3.5 - Applying frequency from the negative portion of a band edge

The frequency chosen in this case is closer to the band edge. As this means it is also closer to the slow lightregion, we expect to see a higher effective index. Furthermore, if we extend (Figure 3.4) for the case where the negative refractive index is higher, we would expect the diffraction angle within the slab smaller resulting in a focused spot that is closer to the slab. This is indeed what is observed in the transmission field distribution calculation in (Figure 3.5).

## 3.3    Simulation for PBG and Negative Refractive Index

We also provide the light propagation through different designed photonic crystals to make sure about what we obtained from MPB. First, we show the typical light propagation through the medium like PhC which the band diagram of mentioned PhC is shown at the (Figure 3.6. a) and also its transmission spectrum for different dimensions in height and width is illustrated in (Figure 3.6.b). In general, flowing light and fluctuation of energy level through the lattice is dependant of geometry and

26

vice versa. In other words, the dispersion diagram shows every single frequency has different type of interactions with the same periodic structures that is computed to obtain its band diagram. Here we intend to study the difference of those computed eigenvalues which is specified for a given structure in (Figure 3.6).

a)

b)

c)
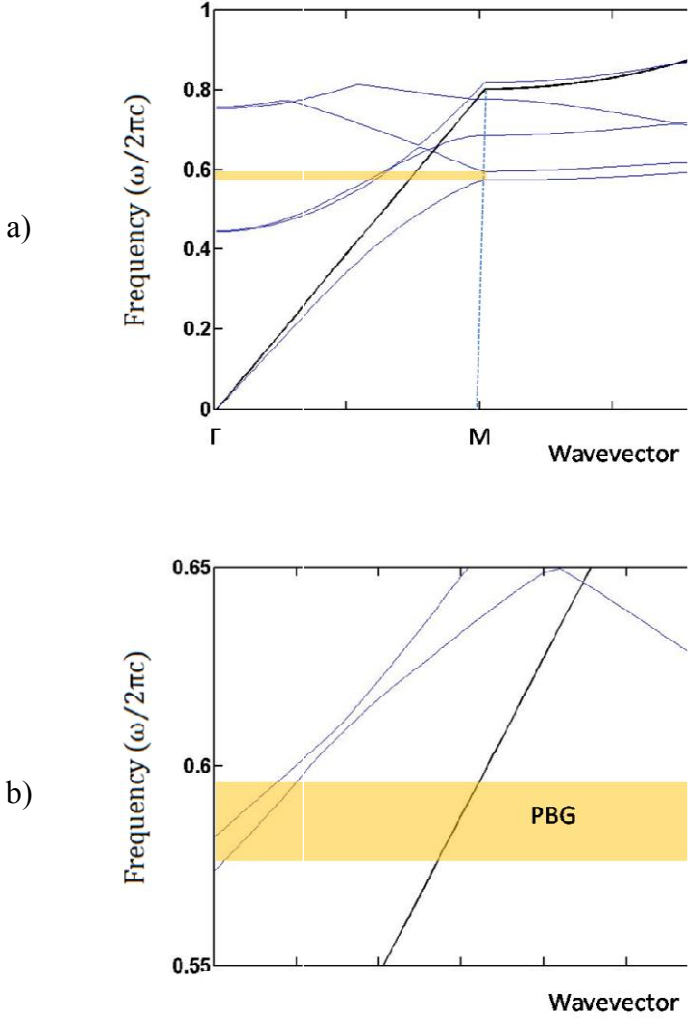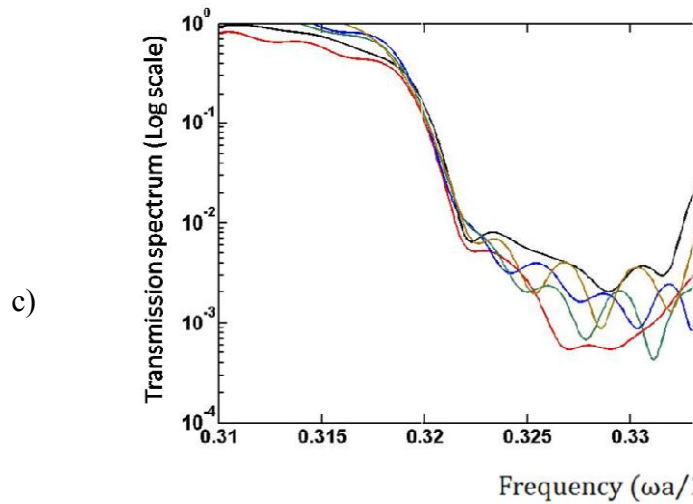


Figure 3.6 - Numerical simulation results of, a) band diagram (3D), b) zoomed band diagram, c) transmission spectra in 2D structure.

Then, we discuss how the refractive index is calculated numerically through the band diagram.

## 3.4    Effective Index

It is a clear concept that light refract through mediums that are allowed based on atomic level of matters. Moreover, the refractive index is geometry dependant which makes designer to manipulate this value according to their aims. However, the concept of effective refractive index explain overall refraction index of a combined material with specific shape and periodicity. Although this concept can be explained from two different points of views that are related to the real and imaginary portion of refractive index, but our case of study has nothing to do with the imaginary portion of refractive index since we are not interested to deal with a mediums to absorb light energy. On the other hand, the real portion of the refractive index represents phase, amplitude and direction of light flow. Therefore, the items that effect a real part of the refractive index can be skimmed in this section briefly. However, this value depends on some parameters like temperature and dielectric but

28

we will examine the wavelength dependency of it. Refractive index of a suggested PhC changes with wavelength that is called dispersion of refractive index. We discuss this dispersion through the band diagram. However, the fact that it is related to the wavelength of applied pulse is also necessary for the sake of clarification. According to the Cauchy's equation [75], refractive index follows bunch of coefficients that is multiplied to the adjacent wavelength of incident that is applied. Meaning that, in reality any incident have a Gaussian spectrum, which appears wavelengths around the central wavelength. Existence of inevitable extra wavelengths in even a small laser pulses bring dispersion relation which is called photonic band diagram. As a result, slope of band diagram or effect of adjacent wavelength determines the effective refractive index of suggested medium. The effective refractive index starts to jump at PBG since the slop of band bending is almost zero and the variation of energy level is about zero with respect to the position in k space. Thus, the enhanced energy is expected around band bending of photonic band gap. In this part we have a plan of studying the effective refractive index in different proposed components that we used to form our suggestion modulated structure besides those that we attached them for the sake of comparison.The effective refractive index of the photonic crystal is calculated from the slope of the band diagram with the following formula [78].

$$v_g = \nabla_k \omega(k) \tag{3.2}$$

, in which the variation of band with respect to the angular frequency gives us the group velocity which contains group of waves and it describe the ratio of the light inside the introduced materials (PhC) with respect to the vacuum and consequently the refractive index value can be computed as well.

### 3.5 Formalism

The numerical results for finding effective refractive index from the band diagrams of 3D lattice that discussed above summarize in (Figure 3.7).

As described in the introduction section of this chapter, obtaining an effective zero index is an important application of the photonic crystals. One of the ways that is used in the literature is to design a superlattice which consists of negatively refracting and positively refracting sections and as mentioned before, negative refraction comes from the photonic crystal and the positive refraction comes from the slab in the example in the literature [80]. Therefore, calculation of positive refractive index for a slab waveguide is presented in next section. Here we are seeing the variation of refractive index versus the angular frequency with which one able to use it to obtain average zero refractive index. We will study this approach at the end of this chapter and the improved version of it in the next chapter.

a)



30

b)
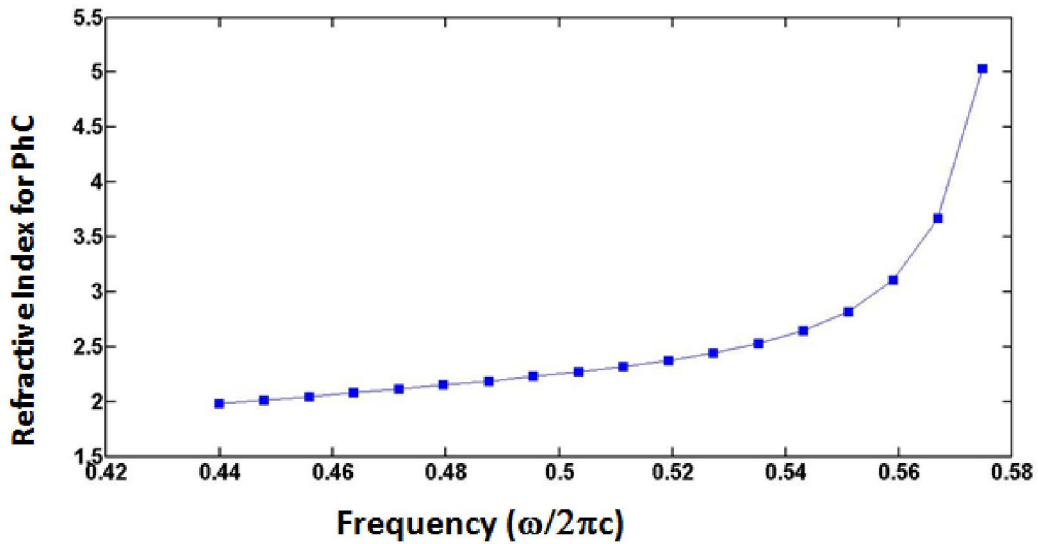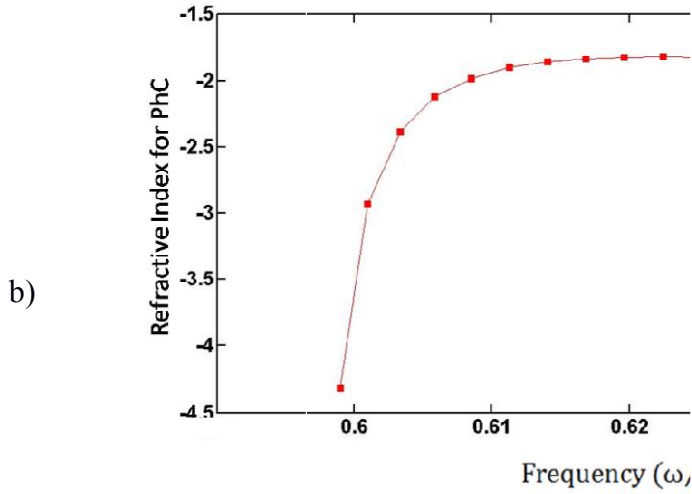


Figure 3.7 - Effective index in regular hexagonal lattice (a) computed from first band (b) computed from second band

## 3.6 Effective refractive index of Slab

The way to compute the effective index of a slab waveguide is a well-known calculation[76] and will be repeated here. The slab waveguide, shown in (Figure 3.8), includes an asymmetric structure including high-index dielectric layer covered on both sides by lower index materials. The slab is assumed to have infinite extensionsin the yz-plane, and defined values in the x direction. In order to compute index of refraction of the slab structure, $n_f$, one should end up with a value that is larger than that of the cover material, $n_c$, or the substrate material, $n_s$, based on having total internal reflection occurrence at the interfaces. By assuming the direction of propagation along the z-axis, the slab is considered within a one-dimensional analysis. In other words, for the sake of simplicity, we are solving a 1D problem but it is directly applicable to many real problems like our case of study in superlattice as the thickness of the slab is much shorter than its width and the length.

31
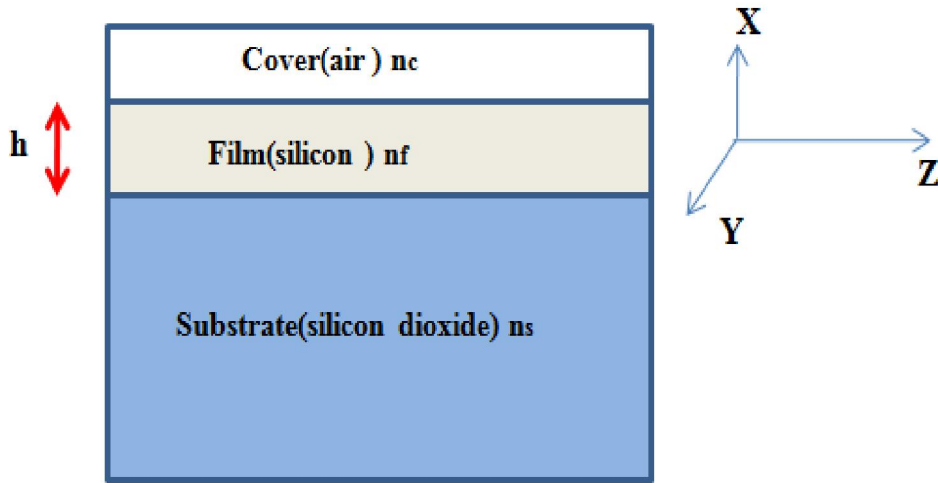
Figure 3.8 - The planar slab (silicon film) on a substrate (SiO2) that have covered with an air layer. The refractive index of three materials is mentioned on its layer

Assuming wave equation in mentioned planar slab is:

$$\nabla^2 E_y + k_0^2 n_i^2 E_y = 0 \qquad (3.3)$$

Based on fixed translational in the z-direction of suggested structure, we ignore the amplitudes of variation along the z-axis, but phase variation is included as below:

$$E_y(x,z) = E_y(x)e^{-j\beta z} \qquad (3.4)$$

Plug in this trial solution into (3.3) and rewrite the equation is:

$$\frac{\partial^2 E_y}{\partial x^2} + (k_0^2 n_i^2 - \beta^2)E_y = 0 \qquad (3.5)$$

By considering, the evanescent light of a coupled field to form a total internally reflected (TIR) wave at an interface the solved equation wave can be either oscillate or decay exponentially.

As a result, for both cases we can re-write the solved wave equation in an exponential form:

$$E_y(x) = E_0 e^{\pm\sqrt{k_0^2 n_i^2 - \beta^2}\, x} \quad, for \beta < k_0 n_i \tag{3.6}$$

Or we can consider it as an exponential decay solution:

$$E_y(x) = E_0 e^{\pm\sqrt{\beta^2 - k_0^2 n_i^2}\, x} \quad, for \beta > k_0 n_i \tag{3.7}$$

In which, we consider $\sqrt{\beta^2 - k_0^2 n_i^2}$ term as an attenuation part of wave:

$$\gamma = \sqrt{\beta^2 - k_0^2 n_i^2} \tag{3.8}$$

Thus, a traveling wave in z direction will have simplified to the equation below:

$$E_y(x) = E_0 e^{-\gamma x} \tag{3.9}$$

According to the (Figure 3.9) we can conclude transverse wave-vector, $\kappa$, as below:

$$\kappa = \sqrt{k_0^2 n_i^2 - \beta^2} \tag{3.10}$$

The (Figure 3.9) the mentioned equation is based on Pythagoras theory that we are using to define both transverse and longitudinal components of light flow.
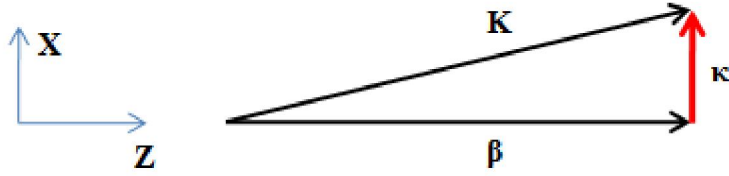
Figure 3.9 - Schematic of wave components where $K = \sqrt{\kappa^2 + \beta^2}$.

Considering a plane wave with two components $\boldsymbol{K} = \kappa\hat{x} + \beta\hat{y}$, and $\boldsymbol{K} = -\kappa\hat{x} + \beta\hat{y}$ with which each k-vector has a plane wave related to wave function. This means that, these components end up with either destructive or instructive interference. Thus, establishments of modes (solutions for β)can be examined through those possible options. However, when the existed modes interfere in a constructive manner, the electric field is in its maximum amplitude, and while destructive interference of existed modes occurs, the intensity reduces to minimum value.

For the TM case, the eigenvalue equation for $\beta$ is [76]:

$$\tan(h\kappa_f) = \frac{\kappa_f \left[ \frac{n_f^2}{n_s^2} \gamma_s + \frac{n_f^2}{n_c^2} \gamma_c \right]}{\kappa_f{}^2 - \frac{n_f^4}{n_c^2 n_s^2} \gamma_c \gamma_s} \tag{3.11}$$

Then the slab structure can be solved through the equation to give the eigenvalues of existed modes inside the waveguide. As a result, we can plug in the results to the equation below to find the effective refractive index:

$$n_{eff} = \beta / k_0 \tag{3.12}$$

Using numerical technique, eigenvalue in (Eq. 3.8),gives us the values of kappa in each crossing point of tangent operator with its equal function graphically. Then, for

each desired spatial angular frequency $k_0$ one can find the propagation constant and follow the (Eq. 3.11) to find out the effective index of engineered structure.

In (Eq. 3.12) consider $k_0 = \frac{2\pi}{\lambda}$ for any particular wavelength. In (Table 3.1), the process of calculating effective index is provided in each row to end up with the last row in which the second row value is extracted from the graphical crossing of (Eq. 3.9) like what is shown in (Figure 3.10).
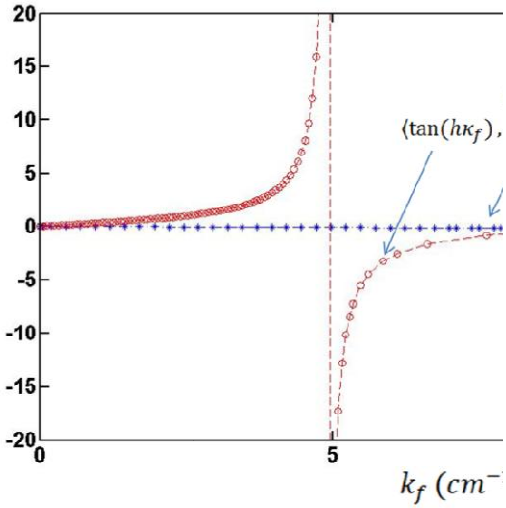


Figure 3.10 - The graphical computation solution to find $\kappa_f$ according to the provided equations

Then, we obtained this numerical calculation through the graphical methods for a range of desired frequencies as below:

35

Table 3-1 - Calculated effective refractive index in slab (silicon) vs. (1/λ)

| $\left(1/\lambda\right)[\mu m^{-1}]$ | 0.61 | 0.625 | 0.64 | 0.65 | 0.665 |
|---|---|---|---|---|---|
| $\kappa_f(cm^{-1})$ | 90700 | 91000 | 91400 | 91500 | 91700 |
| $\beta\ (cm^{-1})$ | 97701 | 101861 | 105873 | 108659 | 109918 |
| $k_0(cm^{-1})$ | 38308 | 39250 | 40192 | 40820 | 41134 |
| $n_{eff}$ | 2.55 | 2.59 | 2.634 | 2.66 | 2.67 |

When we consider the lattice constant and the negative refraction region of the example from the literature (around 0.5 µm, and 0.2875 respectively), it is clear that we need to use the effective index value of around 2.66 for the positive refraction region. In addition, one can simply select the proper values for designing in this range according to what we computed for possible range of frequencies in (Figure 3.11).
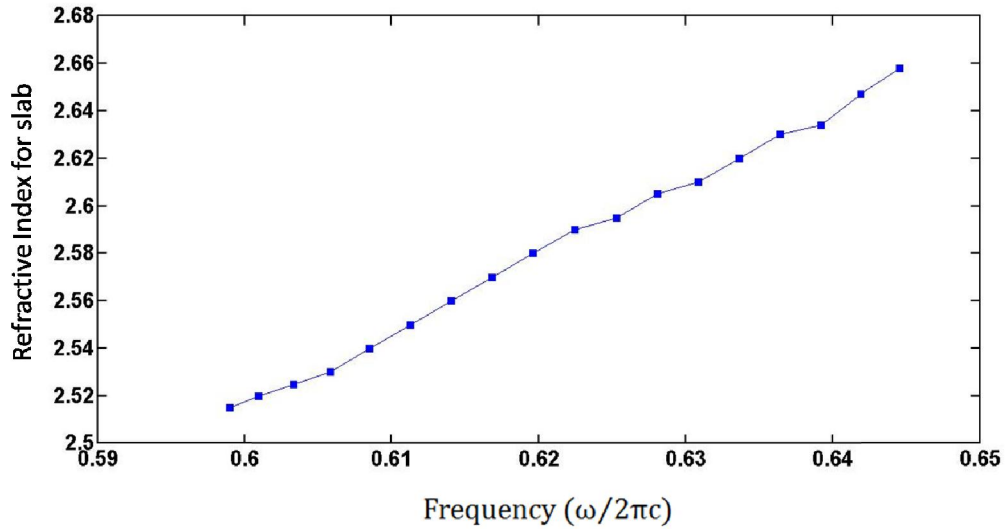
Figure 3.11 - Graphical computation results of refractive index for slab vs. angular frequency.

## 3.7    Constructing superlattice:(Effective refractive index of superlattice)

When we analyze the calculated negative effective refractive index for the photonic crystal structure, we see that the index value is around two before it gets closer to the band edge. On the other hand, we have calculated the positive refractive index for the slab part as 2.66. Therefore, if we combine these two structure in order to form a superlattice that has a zero average refractive index, we need to use a ratio of ($\frac{d_2}{d_1} = 0.65$) in which $d_1$ is the thickness of the photonic crystal part and $d_2$ is the thickness of the slab. In (Figure 3.12) shows what we computed in (Table 3.1) as the dielectric value of slab (silicon film with 0.32 [um] thickness) and the negative refractive index of PhC with the parameters of a = 0.5 [um] as a lattice constant and the radii 0.31 on top of substrate (silicon dioxide with 1 [um] thickness).
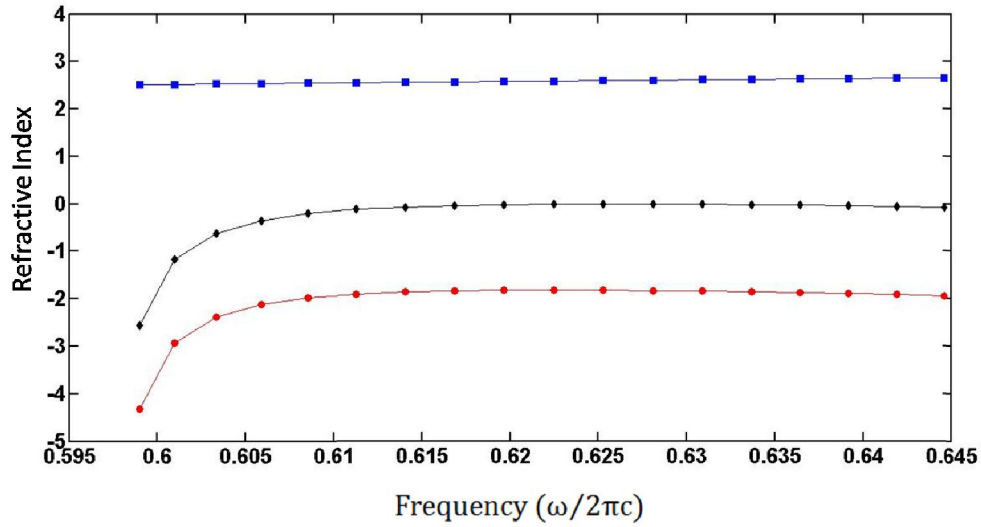
Figure 3.12 - Refractive index profile in slab (blue), PhC (red) and superlattice (black).

In (Figure 3.12) we are seeing the refractive index of a slab that varies gradually with respect to the variation of wavelength. On the other hand, the variation of effective refractive index in small range of frequency is an obvious fact that is shown at the same figure. It is noticeable that combination of mentioned slab with the proposed PhC gives us a unique result that ends up with a zero value of effective refractive index. As it mentioned this result is not only material dependent but also a geometry dependent. Meaning that, the ratio of combination of these two optical components plays major role in determination of having effective refractive index. Applying ($d_2/d_1$) equal to the 0.65 which, determines the ratio of slab layer on PhC thickness, ends up with the zero index of supper lattice around 0.62 [$\mu m^{-1}$].

38
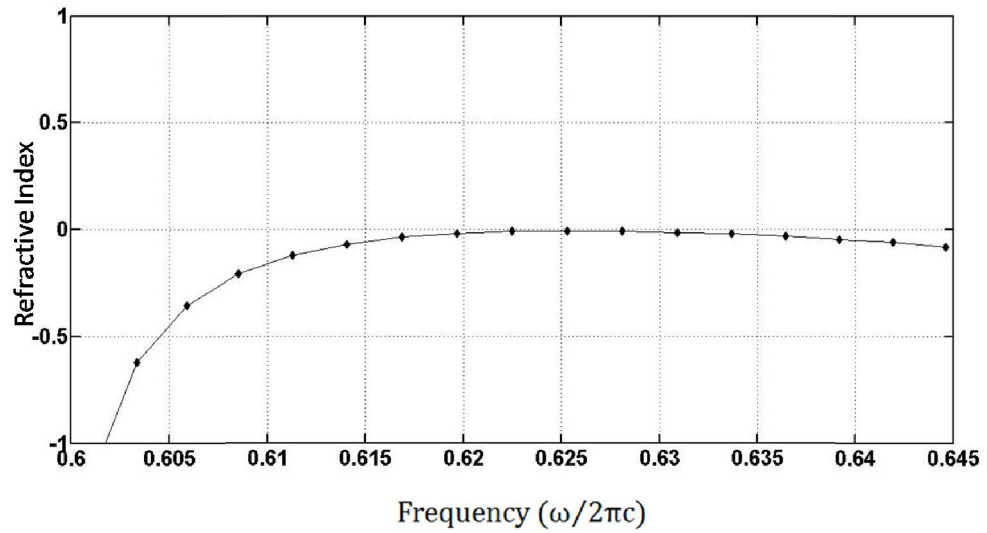
Figure 3.13 - Calculated refractive index in an inhomogeneous superlattice (crystal-slab)with$\left(\frac{d_2}{d_1}\right)$ = 0.65 thickness ratio, where it forms a zero-index with asymmetric refractive-indexprofile.

To have better understanding of proportionality of effective refractive index we changed the ratio of $\left(\frac{d_2}{d_1}\right)$ slightly from 0.65 to the 0.67 and the results of gaining zero refractive index modified as shown in (Figure 3.14).
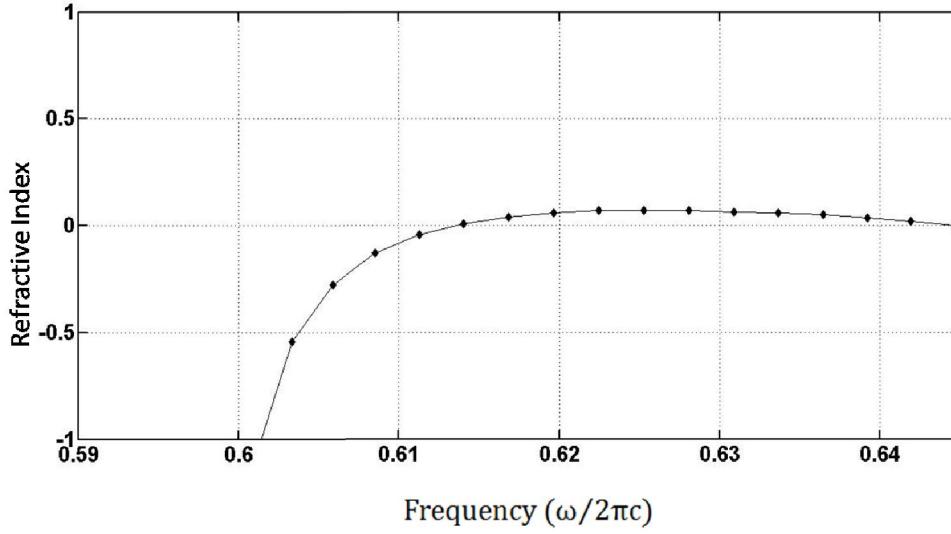
Figure 3.14 - Calculated refractive index in an inhomogeneous superlattice (crystal-slab) with $(d_2/d_1) =$ 0.67 thickness ratio, where it forms two zero-index with asymmetric refractive-index profile.. (delete effective from the graph)

In order to understand what happens theoretically when the average index becomes zero, we also visit the literature [80]. According to the physical origin of the zero- ñ band gap in which the transfer matrix T of the 1D binary periodic superlattice can be concluded through the Bloch theorem [77]:

$$Tr[T(\omega)] = 2\cos \kappa\Lambda \,, \tag{3.13}$$

Where κ is the wave vector and Tr represents the trace operator. For a double layer unit cell we have (3.14):

$$Tr[T(\omega)] = 2\cos\left(\frac{\tilde{n}\omega\Lambda}{c}\right) - \left(\frac{Z_1}{Z_2} + \frac{Z_2}{Z_1} - 2\right) \tag{3.14}$$
$$\times \sin\left(\frac{n_1\omega d_1}{c}\right) \sin\left(\frac{n_2\omega d_2}{c}\right)$$

40

where $n_{1(2)}$, $d_{1(2)}$, and $Z_{1(2)}$ are the refractive index, thickness and impedance of the first (second) layer and ñ represents the average refractive index, $\hat{n}(x) = (1/_\Lambda) \int_0^\Lambda n(x)\, dx$ respectively. In the general case, when $(Z_2 = Z_1)$, if $\{\kappa_0 \Lambda = $ (ñ$\omega$ $\Lambda/c) = m\pi\}$, witch (m) an integer, the relation $Tr[T(\omega)] = \left| 2 + \left( \frac{z1}{z2} + \frac{z2}{z1} - 2 \right) sin^2 \left( \frac{n_1 d_1 \omega}{c} \right) \right| \geq 2 \left|$ holds. This relation clarifies that the dispersion relation has not any real solution for $\kappa$ except $(\frac{n_2 d_2 \omega}{c})$ term should be an integer number times $(\pi)$ that satisfies the Bragg condition. Meaning that, the PBG will form at the corresponding wavelength. However, if the suggested lattice satisfies the special condition of a particularly averaged zero refraction index (ñ = 0), the transmission spectra $Tr[T(\omega)]$ with respect to the given frequency as defined in Eq. (3.14), similarly, get the value higher than two (2). Thus, the imaginary solutions for all $\kappa$ and consequently a spectral gap that is not necessary to be scaled with the given lattice constant of suggested structure will be concluded. This means, we have non-Bragg type gap and it could have a very interesting properties such as zero phase accumulation between various components of the photonic integrated circuits.

We now analyze this non Bragg type novel PBG, namely we change the lattice constant and check the band diagram and the transmission spectrum.

### 3.8 Lattice dependence of the zero-$\hat{n}$ (Band diagram computing of superlattice)

In this section, we provide three cases from what we obtained to admit the calculated transmission spectrum of crystal-slab class of superlattice. Here in (Figure 3.15) the schematic of combination of PhC with slab in which the number of holes in each stack is three and the ratio of thickness is about 0.65. Note that we are considering the PhC zone from the adjacent Gamma in left to the last Gamma at the left side of the periodic holes. Meaning that the length of three holes is 4 times the length

of($a cos\theta$ ) that represents the length of reciprocal lattice in first Brillouin zone of hexagonal lattice.
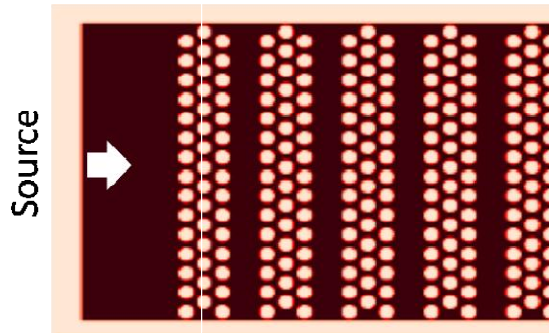


Figure 3.15 - Schematic of Crystal-Slab superlattice with 3 holes in crystal side with 0.65 slab section thickness ratio

In addition, the band diagram of what we are seeing in (Figure 3.15) is attached in the next figure that provides schematic explanation of existence of hexagonal lattice inside the 1D periodic structure of superlattice (Figure 3.16).

The procedure of analysis to this class of band diagram can be described as it is shown in ( ) that the unit cell inside the superlattice contains the multiple irreducible Brillouin zone. As a result, we expect the repeating of computed band diagram for each unit cell while we are traveling through the entire k-space of modulated superlattice. Each minima can be considered as a Γ for hexagonal lattice inside the superlattice and each maxima at the band bending part can be representation of M for the mentioned lattice. By increasing the thickness of alternated lattice inside the superlattice it expects to see more up and down fluctuation of band diagram that will provide in the next cases.
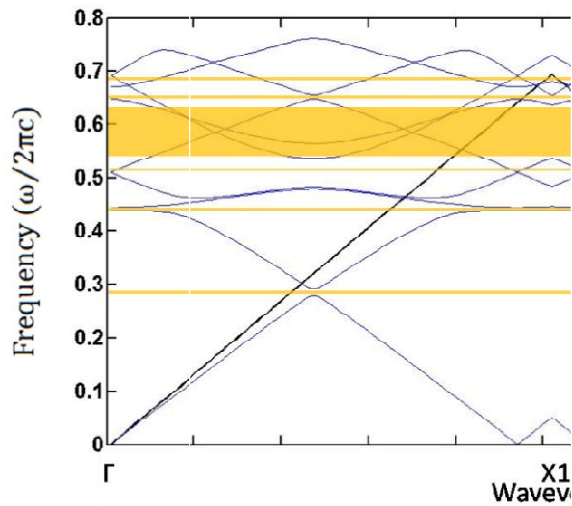
Figure 3.16 - Band diagram of superlattice for 3 holes case.

In addition, the zoomed in portion of what we are interested to illustrate is attached in (Figure 3.17) that clarifies the existence of PBG for the suggested superlattice in (Figure 3.15). The existence of PBG at X1 represents the continuous PBG through the whole lattice in X1 direction. Meaning that, if we compute the transmission spectrum the same reflection spectrum should be seen in the same range of photonic band diagram. In (Figure 3.18) the normalized transmission spectrum is added that is what we expected.

43
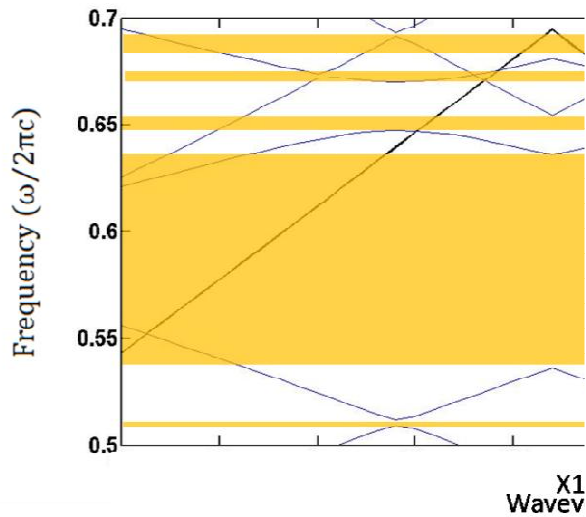
Figure 3.17 - Zoomed PBG superlattice in 3 holes case.

The normalized spectrum of transmission spectra is obtained by dividing the flux values of component at the end of the superlattice to the given Gaussian pulse with a specified range of frequency and finally scaling it in logarithm scale as it is shown in the (Figure 3.18). Note that each decade of Log scale represents 10 percent of reflection of what we applied due to either existence of PBG or specific condition that is dominant in one particular sample of study. It is important to have an accurate examining of transmission spectrum since we want to compare these results with what we have a plan of comparing with the improved one. However, some normalized scales is experiencing extra step of dividing what we explained to gain normalized values to the maximum values of whole data based on showing normalization spectrum at the maximum level of Log scale which is 1 that represent 100 percent transmission. We did not apply this step since we need to show this class of structures experience Fresnel reflection [74], since the combination of introduced elements are not homogeneous. Meaning that, whole structure designed in a way that light experience both Fresnelreflection and the PBG. That is why all transmission

44

spectrum of this type of superlattice are below one (1) normalized spectrum (Figure 3.18).
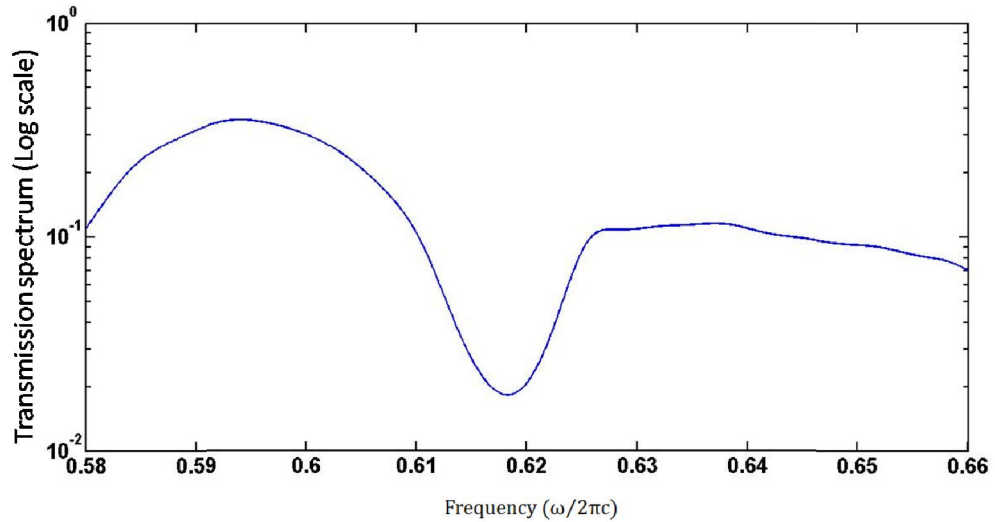


Figure 3.18 - Logarithmic normalized transmission spectrum plotin3 holes case

Again, we are changing the number of holes with the same amount of slab with the 0.65 ratio (Figure 3.19) and start to examine superlattice band diagram and transmission spectra respectively which are attached the results in (Figure 3.20) and (Figure 3.22).

Note that like previous case, we are considering the PhC zone from the adjacent Gamma in left till the last Gamma at the left side of the periodic holes. Meaning that the length of five holes is 6 times the length of($acos\theta$ ) that represents the length of reciprocal lattice in first Brillouin zone of hexagonal lattice.
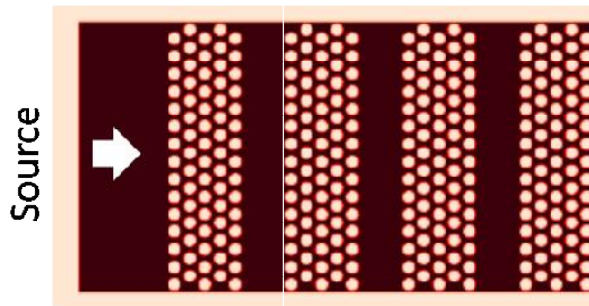
Figure 3.19 - Schematic of Crystal-Slab superlattice with 5 holes in crystal side with 0.65 slab section thickness ratio

(Figure 3.20) is showing band diagram of what is attached schematically as a 1D distribution of periodic superlattice. Since we are interested to examine light flow in X1 direction the computational process is focused on this at the existence reciprocal space. Note that the light line which is shown in each band diagram represents the included k-vectors of computed structure and the eigenvalues are solving through MPB to end up with band diagram structures its own. For example, in this band diagram one simply can figure out that existence of two-dimensional periodicity inside another periodicity parallel to the Gamma-M direction. Thus, the light-line boundary plays a major role in separating the included band diagrams from not included regimes. Unlike the one dimensional structure, the TM or TE mode starts from the beginning of the axis and end in the last computational number according to the given resolution of computation.
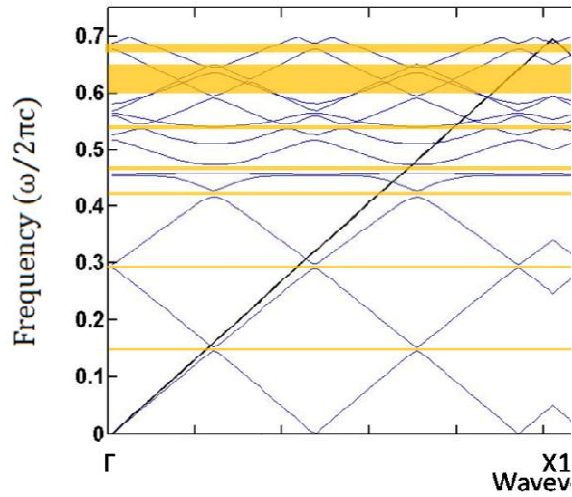
Figure 3.20 - Band diagram insuperlattice for 5 holes case.

The zoomed in portion of superlattice PBG is shown in the (Figure 3.21) that is in total agreement with the transmission spectrum of numerically computed. However, this band diagram provides useful information about the presented structure and it is well clear that there is no need for extending the cell to form a superlattice of complicated band diagram. Since our goal is to approve fixed value of computed wavenumber around $0.62[um^{-1}]$ unlike the scaled method of computing PBG.

47
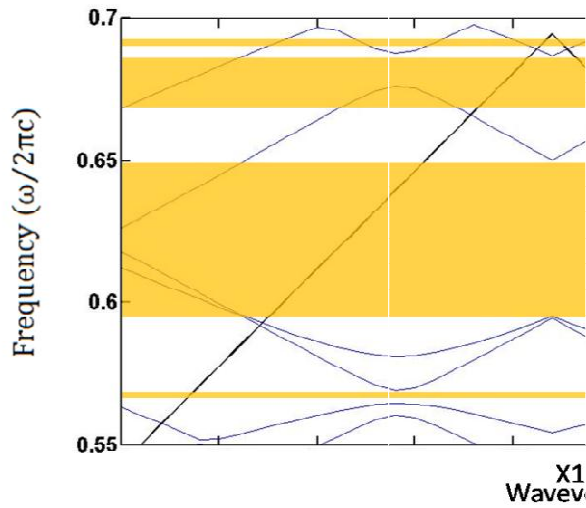
Figure 3.21 - Zoomed PBG superlattice for the 5 holes case

As we mentioned the important part of this study is to remove the low flux volume at the output. By considering the 5 holes case, we are seeing the same problem that the suggested structure deals with is demonstrated in (Figure 3.22). In other words, one can simply conclude that the whole structure has one decade reflection for all applied Gaussian pulse based on Fresnel's reflection light that occurs inside the superlattice and gives rise to destructive interference of coming wave with the reflected light.

48
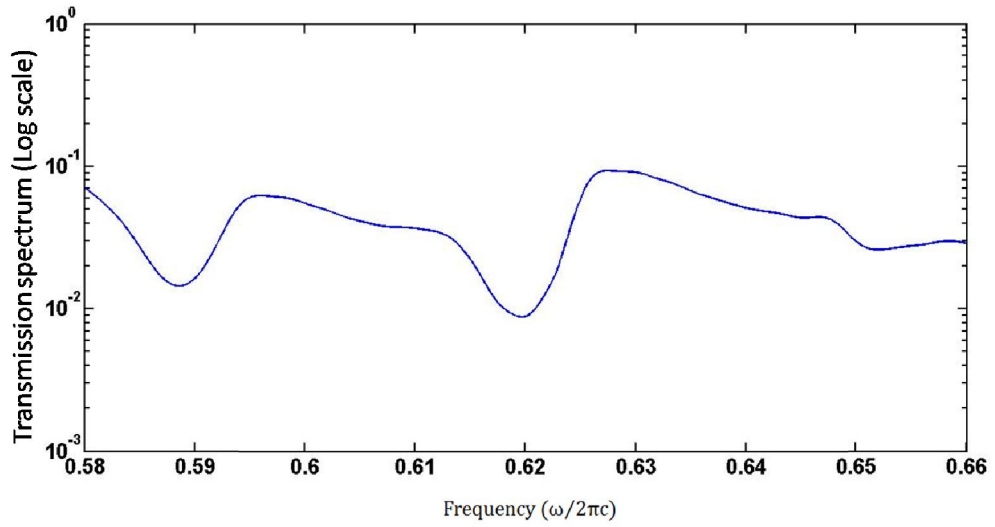
Figure 3.22 - Logarithmic normalized transmission spectrum plotin5 holes case

The Next case is follow the same parameters with the same ratio but in this case we merely increased the thickness of stacks to make sure about the existence of zero-ñ gap based on what we will explain later.
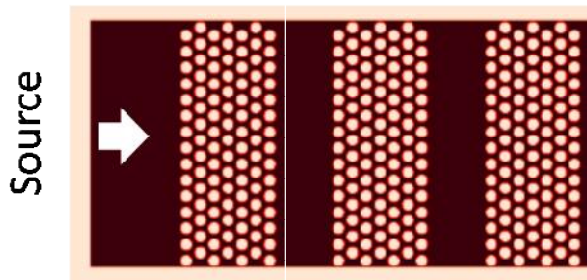


Figure 3.23 - Schematic of Crystal-Slab superlattice with 7 holes in crystal side with 0.65 slab section thickness ratio

49

The result of band diagram for 7 holes cases that is shown in (Figure 3.23) is attached in the (Figure 3.24).
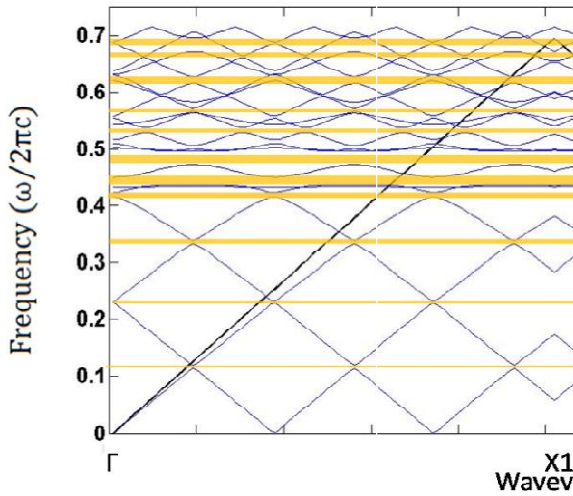


Figure 3.24 - Band diagram of superlattice for 7 holes case. (the orange bar line shows the PBGs)

In superlattice band diagram one might scale the existence band gaps and examine them in transmission spectra but the fact is for zero-ñ gap this is not following since the zeroorder of PBG does not follow the Brag condition anymore. Therefore, exploring any photonic band gap through the band structure is possible to be scaled except for the zero-ñ one. Meaning that, introducing any lattice constant cannot affect the existence of a calculated band gap.

The (Figure 3.25) shows the zoomed in portion of superlattice PBG that we calculated for 7 holes shown schematically in the (Figure 3.23).

50
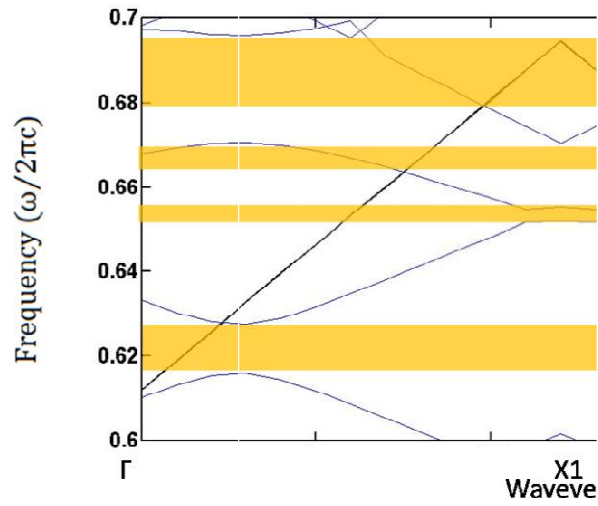
Figure 3.25 - Zoomed PBG of superlattice in 7 holes case

According to the last results, we expect the reflection spectra like (Figure 3.26) with both existence of zero-ñ gap and attenuated flux which implies the destructive interference of travelling wave through the superlattice. The other reflection profiles are based on Brags condition effect that are appears around the desired frequency. We also did simulation of other structures and attached them after introducing the calculation of refractive index which is really essential for understanding of originating zero-ñ gap.
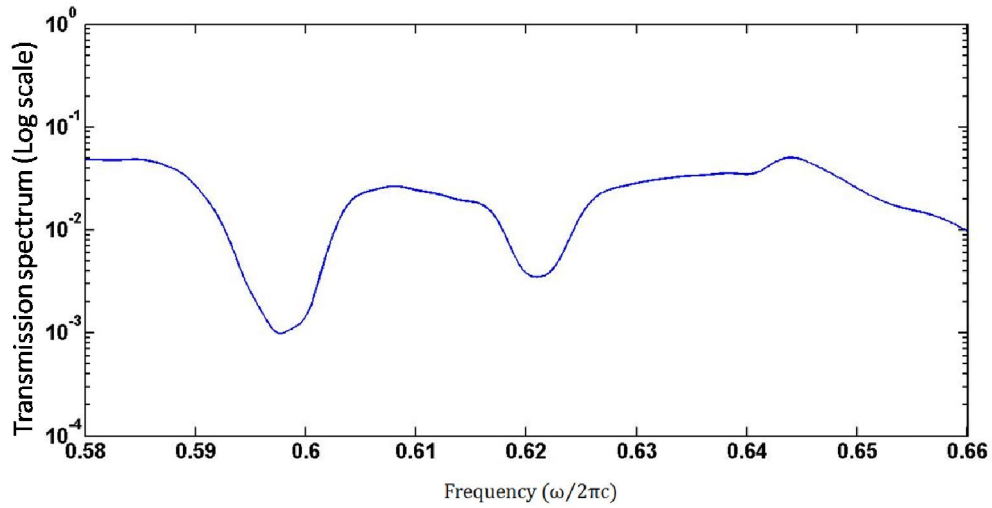
Figure 3.26 - Logarithmic normalized transmission spectrum plotin7 holes case

To conclude what we obtained from three different cases, we can imply to the fixed existence of reflection spectrum at a particular frequency around $1/\lambda \cong 0.62 \ [\mu m^{-1}]$ and consistent of attenuated flux at the output about one decade. The attenuation of signal through the suggested structure can affect the sensor application and signal to noise ratio which is not desired for any optical components. We will provide a solution, by a modulated structure of what is gained through the disordered structure and demonstrate the high transmission spectrum without any attenuation merely by replacing homogeneous component instead of slab.

52
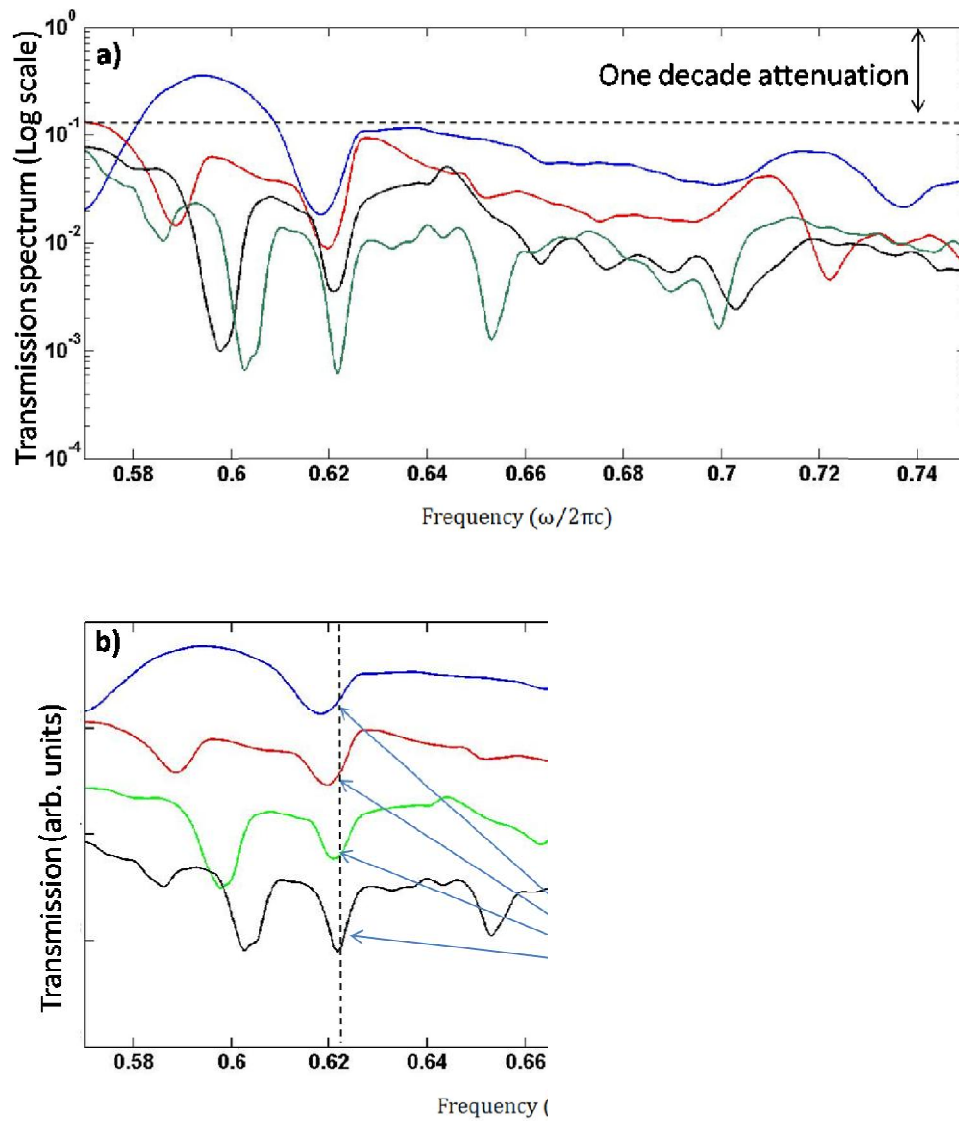
Figure 3.27 - Logarithmic normalized transmission spectrumplotincluding 5 stacks with3, 5, 7 and 9  holes in each stack shows in blue, red, green and black colour, a) Transmission spectrum in log scale, b) the existence of zero-ñ gap gives rise to no shifting in phase

In the (Figure 3.27), we are demonstrate numerically that there exist a zero-$\hat{n}$ gap at $\frac{1}{\lambda} = 0.622$ since the variation of layers in superlattice does not influence the

created gap at $\frac{1}{\lambda} = 0.622$. However, the other spectrum profiles starts to change either to the higher or lower frequencies while the geometry of lattice is changed. This Transmission spectrum shows the existence of zero-$\hat{n}$ gap in a crystal-slab class of superlattice. For the same ratio and the same parameters, we examine the effect of increasing the number of stacks and try it with a longer structure. The results of longer compositions are attached in (Figure 3.28).
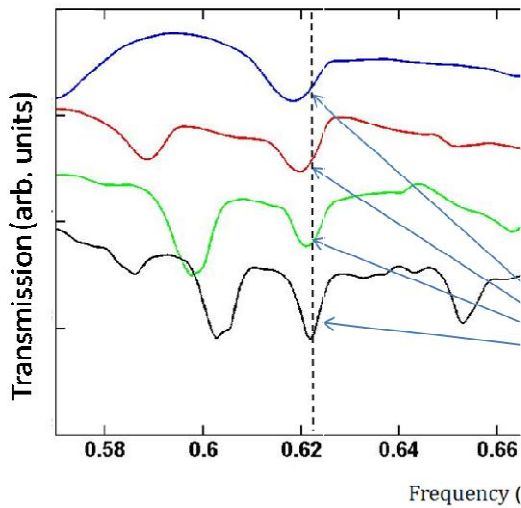


Figure 3.28 - Logarithmic normalized transmission spectrumplotincluding 9 stacks with3, 5 and 7 holes in each stack shows in blue, red, green and black colour in whichthe existence of zero-ñ gap gives rise to no shifting in phase

In the (Figure 3.28), weconclude that the suggested structure is not only suffering from Fresnel reflection (attenuation of signal)but also increasing in length of the superlattice and adding up the number of stacks is not influencingthat much to have deep of stop band and efficient contrast and applicable in switching components of PIC type of devices.

54

# CHAPTER 4

## 4 RESULTS AND DISCUSSION

In this chapter, we will study the effect of disorder on the band diagramofPhCsand will apply it to form a superlattice. In addition, it will open new options of controlling light through the designed complicated lattices. The aim of this approach is to have deep understanding of changing density of states inside the lattice and realize proportionalities of effective refractive index with introduced dielectric while we are modifying the density of certain dielectric with respect to the regular structure. We suggest a disordered modulated hexagonal structure in which the position of holes varies in a paralleled direction of applied light direction and study, with numerical methods and simulation, its influence on both effective refractive index and photonic band gap. Fortunately, the results of this approach are promising enough to utilize it in various applications of on-chip integrated circuits. Therefore, we obtained new version of modifying PBG, swinging PBG to either high or low level of frequencies, that is obtained simply by modifying the geometry of traditional hexagonal without altering any other parameters. We applied this class of suggested structure in one particular superlattice to gain zero-$\hat{n}$ gap for the sake of comparison with the reported structures recently [80]. However, self-collimation is an interesting topic of PhC field but the challenging matters in this path made it the less affordable results [81] for mass production. However, previous results are suffering from energy losing since the modulated PhC, square lattice with Dirac cones band diagram, has utilized metallic material inside the lattice. In this set of computation, we brought two types of suggested Supperlattices together to have clarification of difference between them. In addition, we are trying to form a broadband zero-$\hat{n}$ gap with lossless energy and improve the reported experimental results recently [82]. We also added some unsteady simulation of proposed

structure about E-field distribution to acknowledge our computed results with Meep and MPB.

## 4.1    Photonic Band diagram

The photonic band diagram of regular hexagonal is shown in (Figure 4.1), and its zoomed in figure is attached to give more details about the existence of band gap at the Γ-M direction between first and second band diagrams. In addition the geometry of suggested regular hexagonal include 0.5 [$\mu m$] lattice constant with the 0.32[$\mu m$]film of silicon on top of 1[$\mu m$] substrate which is silicon dioxide. The (r/a) is 0.35 with the cylindrical holes that have the same height of film (silicon).
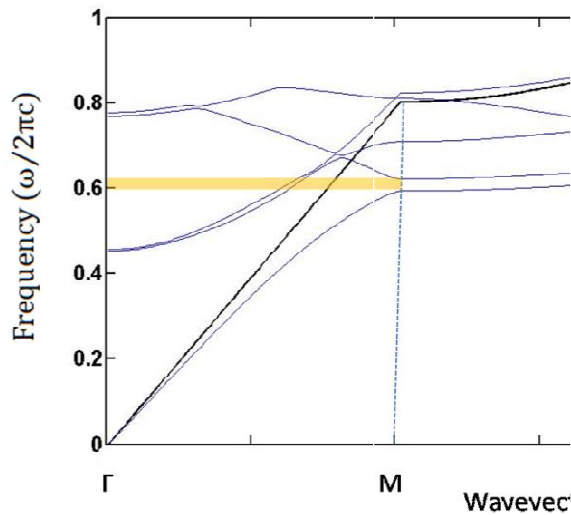


Figure 4.1 - Photonic band diagram in regular hexagonallatticewhere lattice constantis 0.5 [$\mu m$], and 0.32 [$\mu m$] silicon film thickness on a 1[$\mu m$]thickness silicon dioxide substrate. with (r/a = 0.35)
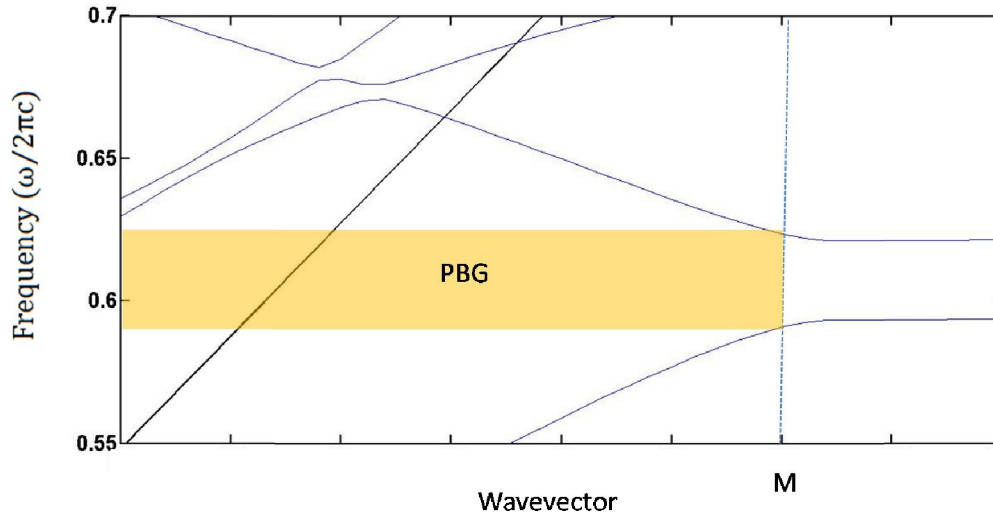
Figure 4.2 - Zoomed section of photonic band diagram with PBG in Γto M direction

In order to have different PhCs with different characteristics, there might be many methods of modifying such as changing radius, lattice constant, thickness and even type of lattice like hexagonal, square and triangular and so on [69]. However, we study hexagonal structure without changing any other parameters to produce both positive and negative refraction indexes in the range of 1500 ~ 1600 [nm] wavelength. This variation is based on reducing the angle of Γ-M & Γ-K direction, However, it is a new type of disordered hexagonal structures which are enormously useful for on-chip 2D devices. This new type of PhCs helps to have a broad manipulation range of complicated superlattice since this modification gives rise to swing PBG. In other words, this type of disorders provides broad options with expected results of designing and efficient constituent. The variation of angles can be accomplished by means of shifting holes in either x-axis or y-axis and even it is possible to change it in both axes simultaneously. Here we showed in (Figure 4.3) the variation of angle by shifting in X-axis with fixed length of Y-axis, since we are interested to examine variation of PBG in M direction (X-axis). As a result, the whole lattice will have fixed width of lattice beside the same applied parameters such as thickness and radii for the regular PhC. In (Figure 4.3) the

changing parameters in both Cartesian and K space are clarified with some other details.in (Figure 4.4)
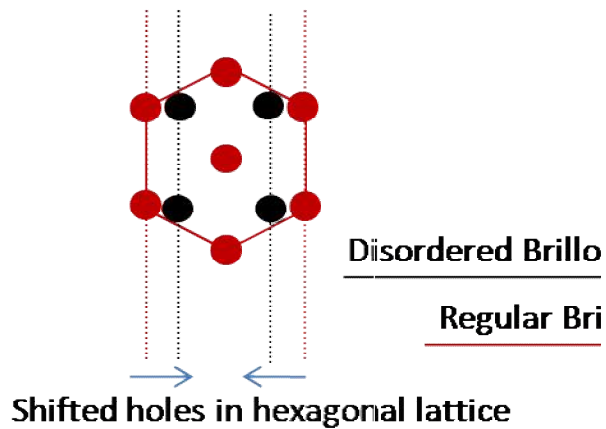


Figure 4.3 - Schematic of shifted structure from regular position (red) to the new disordered position (black)where the black holes generate new Brillouin zone.

This modulation that is originated from the disordered theory can be explained in another fashion. By assuming the holes (cylindrical air) inside the lattice with a particular dielectric, one can simply mention the density of state to examine effect of manipulation of PBG by fluctuating a particular density of dielectric inside the lattice. In our case of study, the increasing mentioned angle ends up with the compression of holes and finally increasing lower dielectric state inside the silicon with higher epsilon.
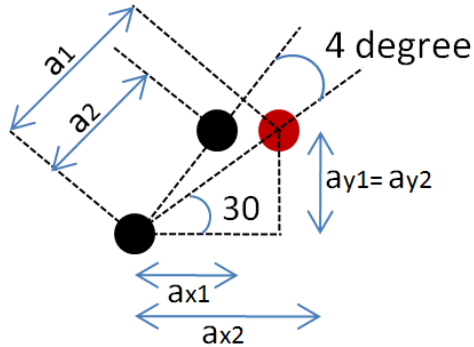
Figure 4.4 - New parameters for disordered hexagonal structure after shifting in X-axis.

In (Figure 4.4) the result of disordered well explained that causes the compression of holes inside the lattice. Since we are studying the effect of this phenomena numerically, existence of two lattice constant might be a little confusing. However, the lattice constant is considered according to the regular hexagonal structure since the determination of film thickness and even substrate is computed according to the regular hexagonal structure. Meaning that ($a_1$) as a regular lattice constant determines the thickness of silicon film and substrate not ($a_2$) which is coming from the disordered effect. For example, for our computation of band diagram the scaled parameters (h/a) , (r/a) are 0.64 and 0.35 which gives us $0.32[\mu m]$ thick silicon and $0.175 [\mu m]$ radius of holes if the lattice constant get the value of $a_1 = 0.5 [\mu m]$.

In (Figure 4.5) the computed band diagram of all angles is shown all together for the sake of clarifying swinging PBG with disorder effect. However, the first and second bands of applied parameters (r/a=0.35, thickness of silicon=0.32 $[\mu m]$ and constant thickness of substrate) creates photonic band gap at certain range of frequencies with different lattice geometry. In other words, variation of angles starting from 28 degree to 34 degree gives rise to modification of lattice constant but with fixed width of previous structure. However, reducing the angle of $\Gamma$-M and $\Gamma$-K direction gives rise to increasing of lattice constant and shifting the PBG to the lower frequencies. Moreover, increasing

59

the mentioned angle makes reduction of lattice constant and shifting of PBG to the higher frequencies. The reason of rising first band in the band diagram is due to increasing the density of lower epsilon (air) at the same geometry which gives rise to enhancing the energy level at higher band because of large tendency of photons to flow in high refractive index. The (Figure 4.5) illustrates the reduction of lower dielectric density at higher degrees of disordered $\theta > 30^o$ between Γ-M and Γ-K in hexagonal lattice.
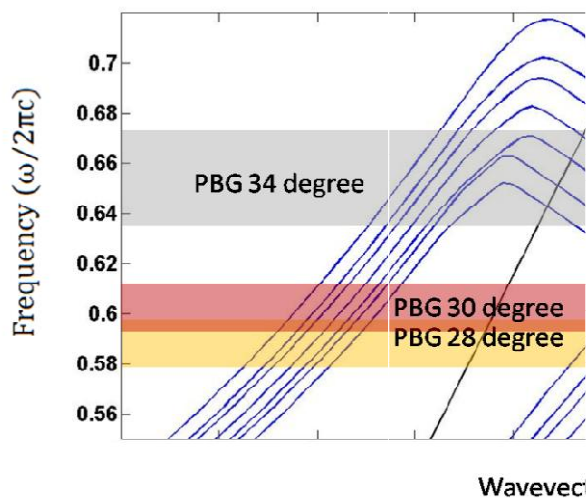


Figure 4.5 - Zoomed portion of band diagrams for PhCs with different angles between Γ-M and Γ-K direction. Increasing the angle gives rise to increasing the PBG and swinging it to the higher angular frequencies, (orange bar line) shows the PBG range for 28 degree, (red bar line) shows the PBG range for regular lattice, (gray bar line) shows the PBG range for 34 degree

In (Figure 4.6.a), (Figure 4.6.b), (Figure 4.6.c) the procedure of variation of density of states is illustrated by changing the order of disorders, which is discussed already.
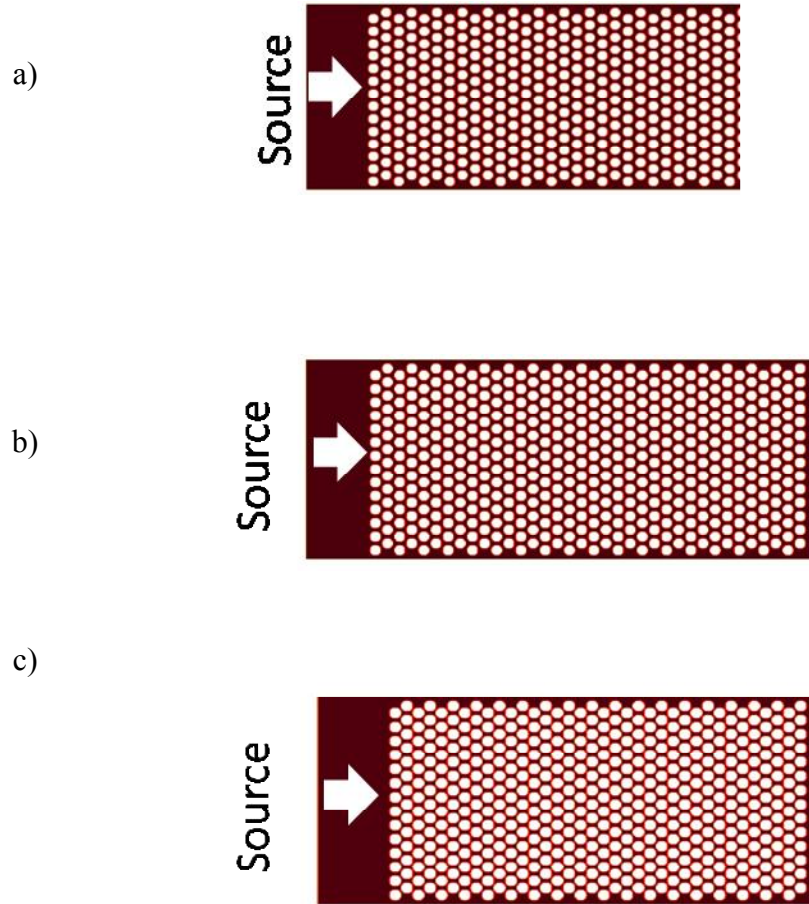
Figure 4.6 - Angle variation effect in hexagonal lattice on lower dielectric density inside the lattice, a) 28 degree, b) regular hexagonal with 30 degree, c) 34 degree.

For example if one needs to have a PBG at higher frequencies it can be realized merely by increasing the lower dielectric (real part) like what is shown (Figure 4.6) in which all parameters are the same as regular hexagonal structure but the degree of disordered increased from 30 degree to the 34 degree.

We also did simulation of transmission spectrum, using FDTD in Meep, to examine results of computed photonic band diagrams in (Figure 4.5). According to the normalized spectrum of transmission versus frequency in (Figure 4.7) the PBG is

swinging and it is in complete agreement with the transmission spectrum results. As a result, this new class of disorder in hexagonal structure provides complete manipulation of PBG, negative/positive and even combination of different types with each other to gain so many complicated approaches.
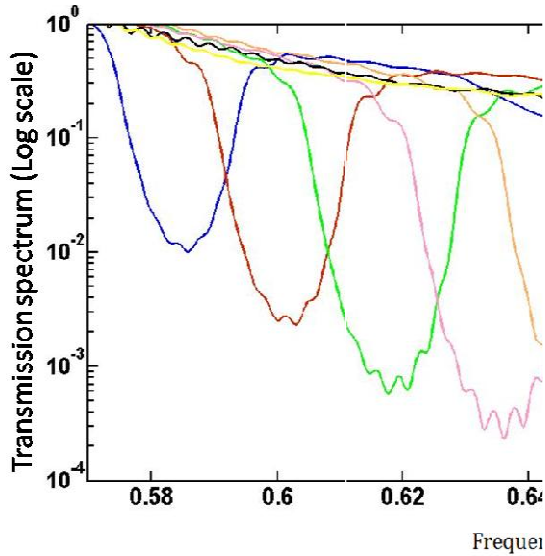


Figure 4.7 - Logarithm Scale of transmission spectrum of different PhCs

## 4.2 Superlattice PBG calculation of Crystal-Crystal

We discuss the superlattice of crystal-crystal band diagram which is provided in (Figure 4.5).Therefore, we expect multiple dispersion alternation values in one superlattice since it is not irreducible zone to one portion of included unitcells. However, before examining the agreements of both transmission spectrums with the superlattice band diagram we need to know:

In first case, we start with the three holes in each alternating layer as it is shown in (Figure 4.8) that is the smallest modulated of our investigating.
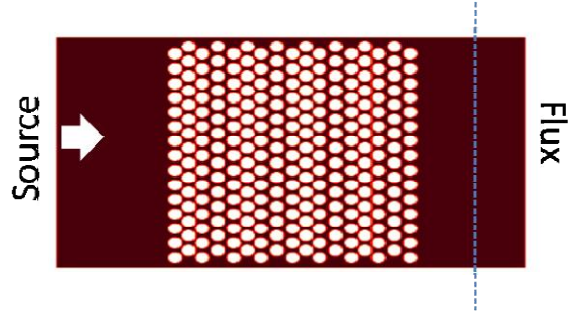
Figure 4.8 - Schematic of Crystal-Crystal superlattice with 3 holes in each side where one column of holes (air) is in common for both sides.

According what we discussed in third chapter the computed band diagram of superlatticeis computed only in x1 direction since we are interested to see the effect of disorder in Γ-M direction and our computed PBG for the regular crystal is in this region too.
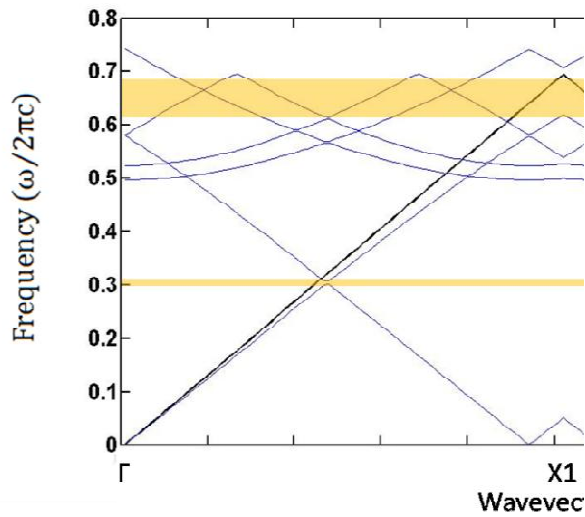


Figure 4.9 - Band diagram of superlattice for 3 holes (crystal-crystal) case.

The zoomed in part of computed band diagram is attached in (Figure 4.10) clarify existence of both zero order gap and those which are following Bragg condition. One can simply can take a frequency from those bands and scale it to estimate the range of stop band in transmission spectra. One of the advantages in designed structure is that

there is no necessity for scaling step. In other words, the existed PBG in the band diagram can be explored in the transmission spectra directly without scaling.
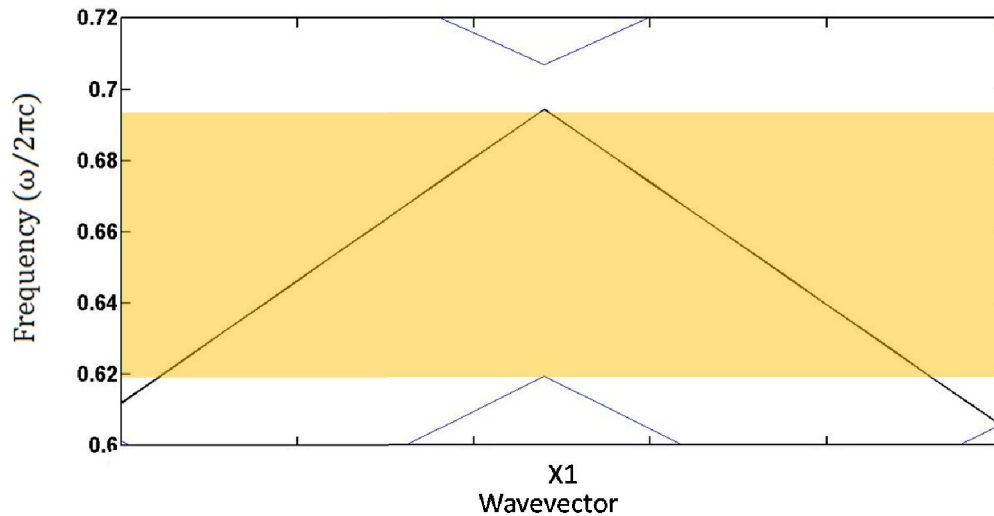


Figure 4.10 - Zoomed PBG of superlattice (crystal-crystal) in 3 holes case.

The transmission spectrum of what we introduced is shown in (Figure 4.11) in which the normalized spectra shows no attenuation of applied signals at the output of superlattice structure. Thus, the computed flux is almost higher than the previous case that is addressed in last chapter.
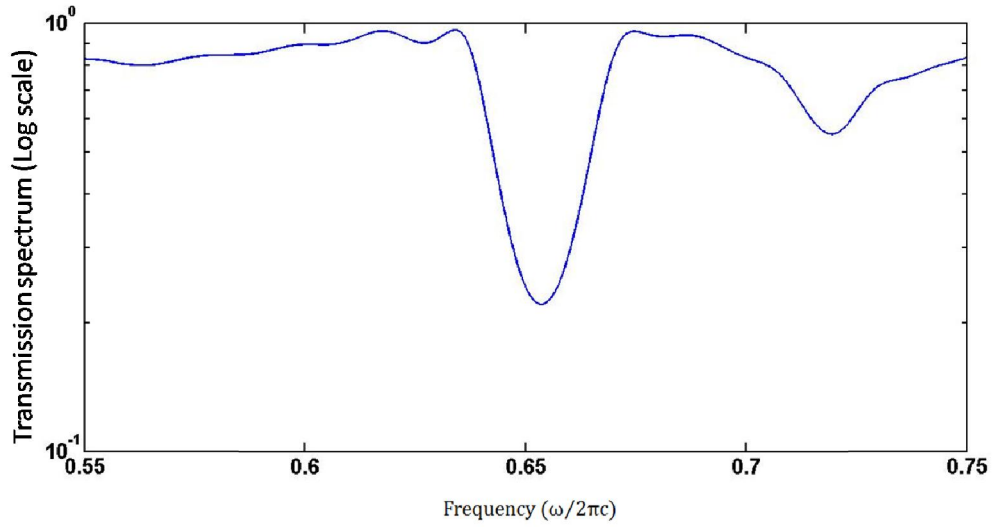
Figure 4.11 - Logarithmic normalized transmission spectrum plotin3 holes case

For thicker layer we increased the number of holes in each side and produced 5 holes in each section of PIM (disordered lattice with 34 degree) and NIM (regular lattice with 30 degree) in which the one column is in common (Figure 4.12).
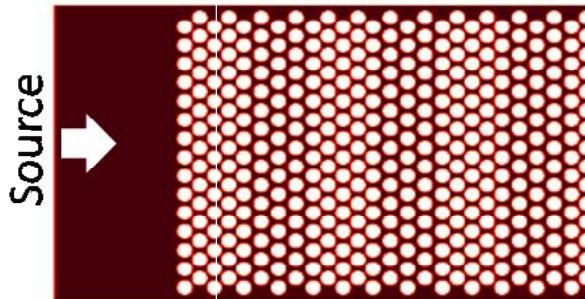


Figure 4.12 - Schematic of Crystal-Crystal superlattice with 5 holes in each side where one column of holes (air) is in common for both sides.

For the shown schematic we compute the band diagram and it is shown in (Figure 4.13) for more details it is zoomed in (Figure 4.14).
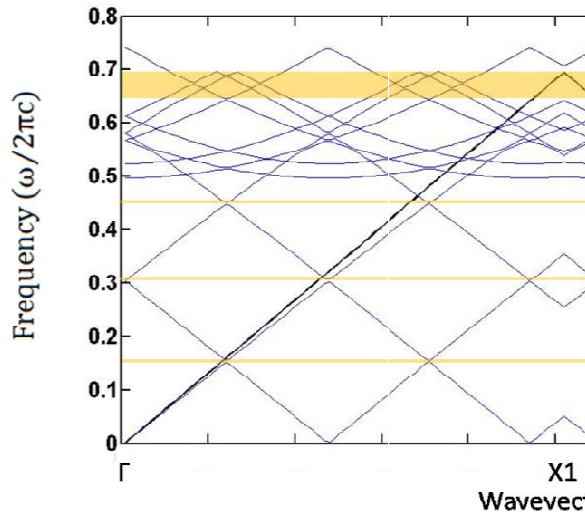
Figure 4.13 - Band diagram of superlattice for 5 holes (crystal-crystal) case.

Zoomed inpart of what we need to observe as a superlattice band gap is attached in (Figure 4.14). The transparent band shows whole reflected spectrum but except the zero-ñ gap the other frequencies should be scaled to follow the Brag's gap based on finding the same computed PBG in the transmission spectra. Thus, the illustrated frequency around the 0.66 $[um^{-1}]$ is not required to be scaled since it is absolute zero order of gap which is discussed in (Eq. 3.14).
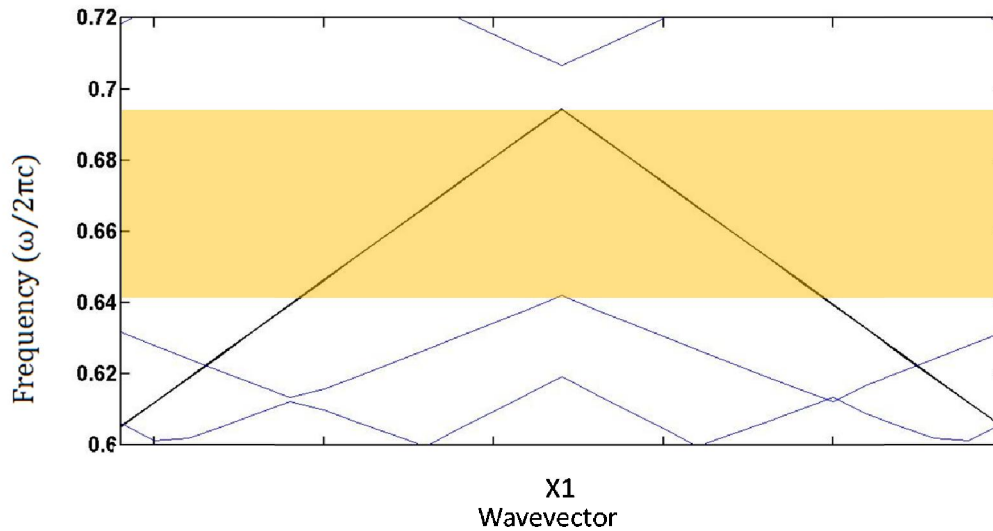
Figure 4.14 - Zoomed PBG of superlattice (crystal-crystal) in 5 holes case..

Transmission spectrum for the case of 5 holes admit the computed superlattice band gap which is shown in (Figure 4.15) and admit the existence of fixed gap with a symmetric profile of refractive index. One can simply, compute either by scaling the computed band diagram from (Figure 4.14) and see the result in transmission spectra or for zero-$\hat{n}$gap it is realized by comparing the computed frequency range in the band diagram with the same value of stop band at the transmission spectrum in (Figure 4.15). Perhaps, to compare with the other cases this thickness has a good contrast of comparing signal, transmitted frequency near the gap, to the gap transmission power. In other words, the logarithm scale of what this case provides is desirable to use for example in a switch components of PIC.
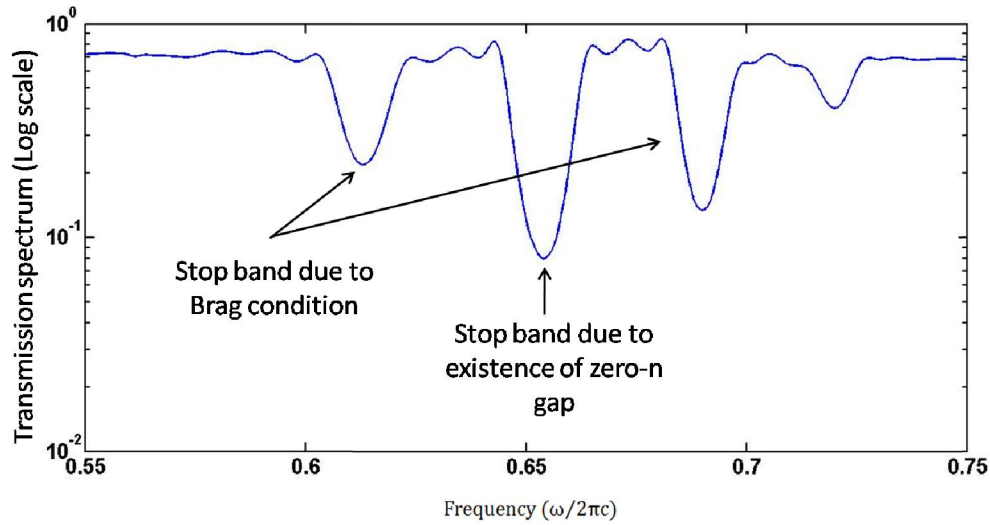
Figure 4.15 - Logarithmic normalized transmission spectrum plotin5 holes case

In third case we have 7 holes in each section of both positive and negative layers and one column of holes are common in between. Meaning that, the seventh column in the first layer (PIM) is belonged to both sides of the stack. The ration of these thickness is designed in a way to form a equal number of holes in both sides to end up with the zero-ñ gap profile at the desired frequency. In other words, the ($\frac{d_2}{d_1} = 1.1$) in which the d2 is the negative layer's thickness with a regular hexagonal structure and the d1 is the thickness of disordered hexagonal layer with a negative value of effective refractive index. Note that, the mentioned ration is equal to ($ax_2/ax_1$) so increasing the number of holes has to be the same. Thus, we will have the equality of number of holes in each side to form a superlattice to gain zero-ñ gap.

68
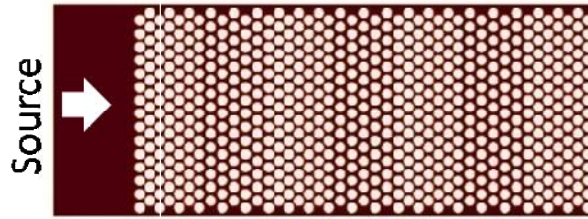
Figure 4.16 - Schematic of Crystal-Crystal superlattice with 7 holes in each side where one column of holes (air) is in common for both sides.

Following band structure in (Figure 4.17) shows so many fluctuation of bands since the computed cell contains multiple reduced Wigner-Seitz cell that gives rise to having multiple k-vectors through the superlattice k-space.
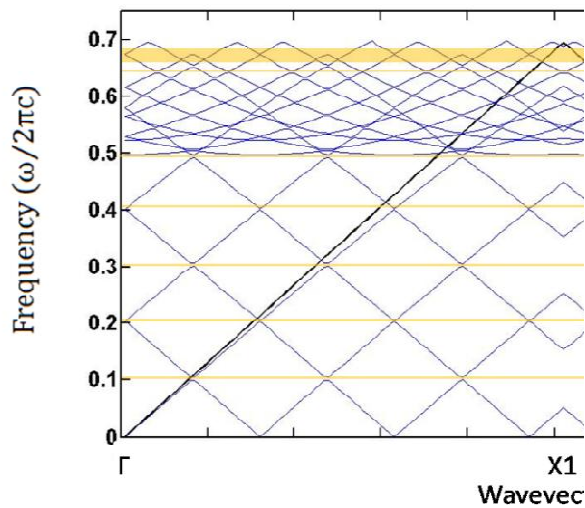


Figure 4.17 - Band diagram of superlattice for 7 holes (crystal-crystal) case.

In addition, in (Figure 4.18) the zoomed in section of superlattice PBG is shown with a gray band. As it is clear from the figure the reduction of one particular band of frequencies due to increasing the thickness of the structure which gives rise to narrowing of the superlattice PBG.

69
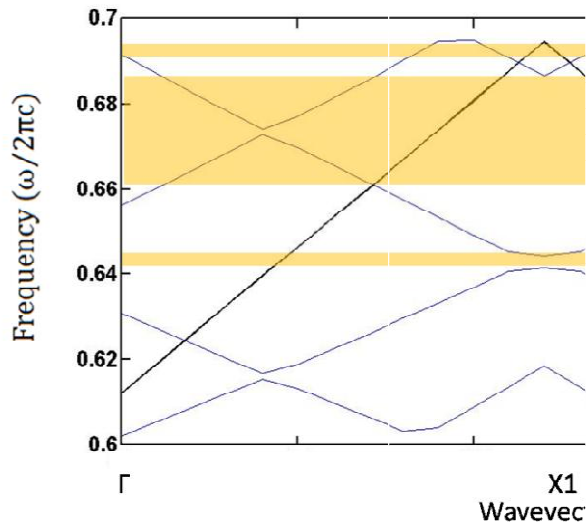
Figure 4.18 - Zoomed PBG of superlattice (crystal-crystal) in 7 holes case.

The transmission spectrum includes this PBG and the variation of other Brag's gap should be defined through the scaled calculation. For example, any selected gap frequency according to the band diagram structure should be multiplied to the superlattice constant and divided by the suggested lattice constant to figure out which wavenumber should be resonate as a gap in transmission spectra.
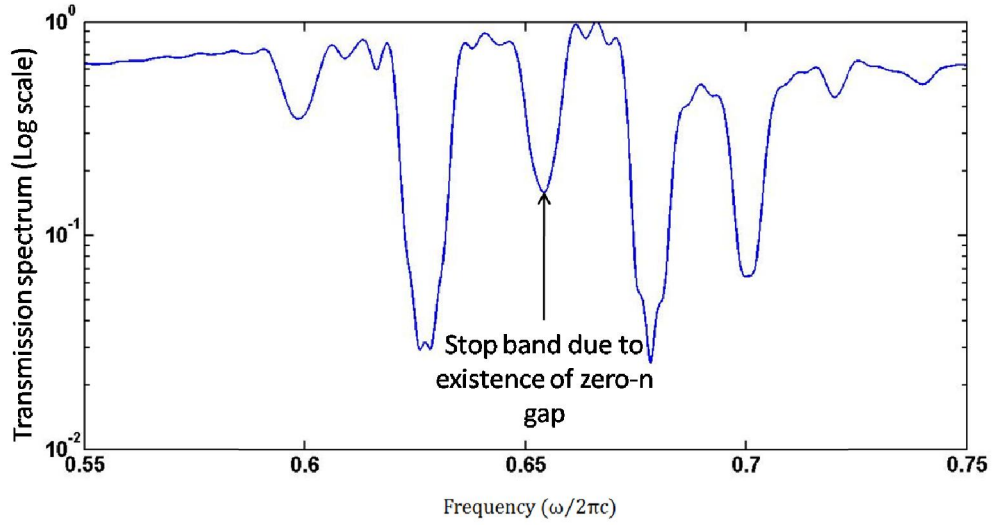
Figure 4.19 - Logarithmic normalized transmission spectrum plotin7 holes case, the importance of stop band due to the existence of zero-$\hat{n}$ gap is clear since it is not shifting by changing the structure.

Consequently, all selected cases admit the existence of PBG at the same range of frequencies that proves zero-$\hat{n}$gap at (1/$\lambda$ =0.655). In this set of calculation we assume the lattice constant as a function of disorder, however, it is determine from the thickness of the film (silicon) which is computed to the regular one. Therefore, the lattice constant has not to be changed for computation process since the thickness of silicon is the same through the lattice either it is regular or disordered region. It is noticeable that the rough value of (a = 0.511) is for the sake of computing in range not in exact value of zero-$\hat{n}$gap. In other words, it is also possible to recalculate the 1/$\lambda$ with (a = 0.5) for any frequencies included in superlattice band diagram and illustrate the existence of fixed gap in broad band. In addition, we provide the both band-diagram and computation of crystal-slab type, which we showed in previous section.

## 4.3 Effective refractive index of Crystal-Crystal superlattice

As we discussed the importance of the band diagram in previous chapter and the effect of changes of band diagram with respect to the k-space variation. Here we provide the numerical results of finding effective refractive index with respect to the slop of both

71

light line and band diagrams. First, we compute the refractive index of regular hexagonal PhC around the PBG.
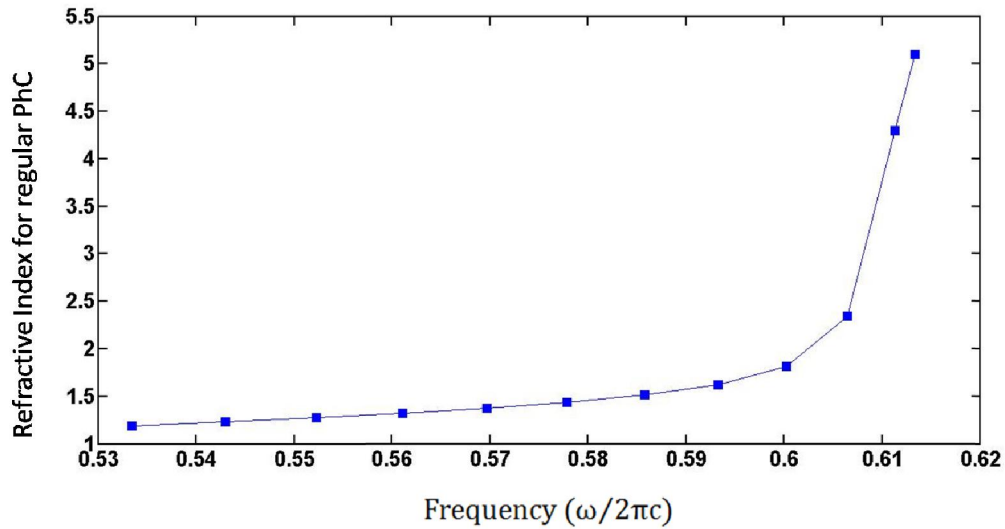


Figure 4.20 - Refractive index vs. angular frequency

In (Figure 4.20) the refractive index of regular hexagonal lattice calculated through the (Eq.3.10) for first band. Moreover, it is applied to the second band and the results attached in (Figure 4.21) in which the negative values of refractive index versus angular frequency are gained due to negative slop of second band with respect to the k-vectors in band diagram.
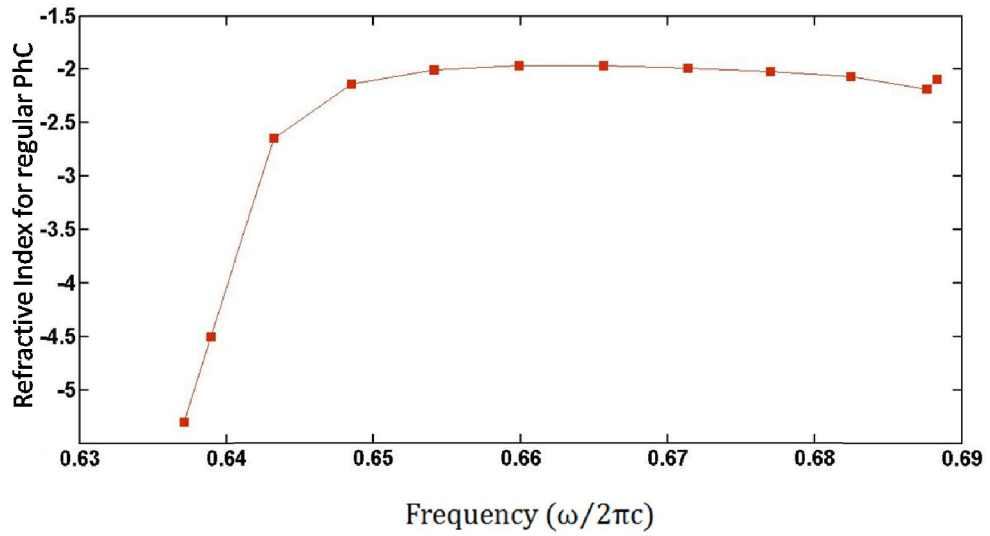
Figure 4.21 - Refractive index vs. angular frequency

Second, the calculation of refractive index in disordered hexagonal structure in which the density of lower epsilon is increased with respect to the regular one. In other words, the first band which represents the lower epsilon and second band which represents the energy level of higher epsilon shifts in upper states due to increasing density of lower dielectric inside the PhC. (Figure 4.22) shows the creation of sharp slop with enhanced refractive index around the band gap.

73
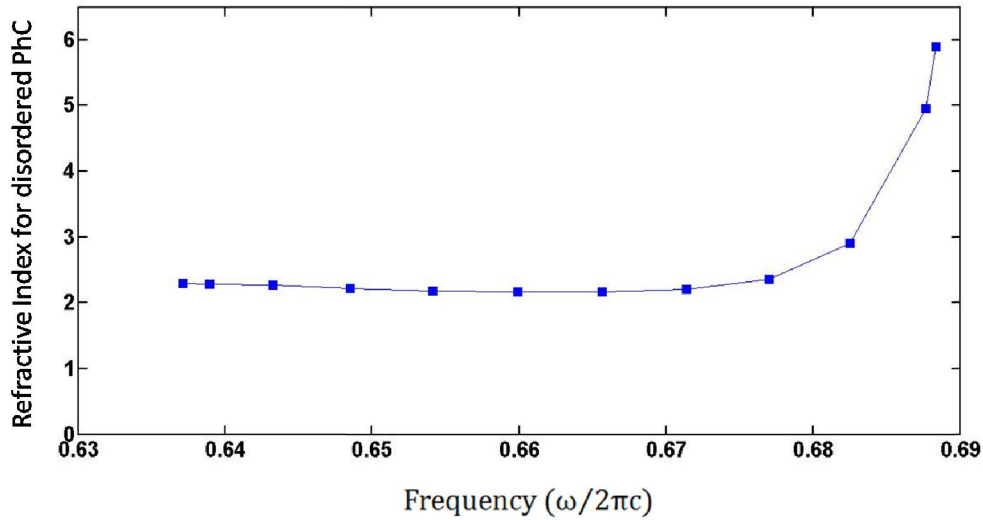
Figure 4.22 - Refractive index vs. angular frequency

Moreover, we compute the second band slop and plug in the (Eq.3.2) that gives us the results of (Figure 4.23) in which the negative values of refractive index versus angular frequency is shown. The same approach for gaining zero average is realized by accurate calculation of these two different index value including negative and positive. Consequently, the ratio of combination will help us to manage the suggested component to have a crystal-crystal superlattice that has useful advantages over the last structure. We will examine these priorities after computing the index values of first and second band diagram which gives positive and negative value due to their slope effect on group velocity respectively.
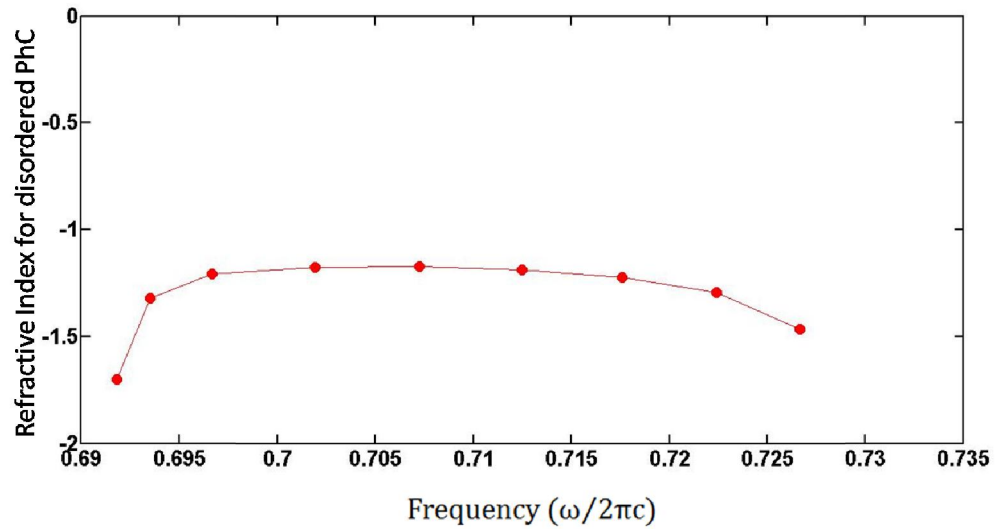
Figure 4.23 - Refractive index vs. angular frequency

In addition, the combination of two types of crystals, regular and disordered, gives rise to obtain almost zero index around the normalized frequency of $(1/\lambda = 0.655)$.

As it is seen from the computed values in (Figure 4.22) this values are proper to use them with mentioned ratio NIM over PIM in which the positive layers have comparable values with the NIM structure. In other words, the regular hexagonal lattice has suitable negative values at the same range of frequency that the disordered one (34 degree) give us with mentioned process of calculation.
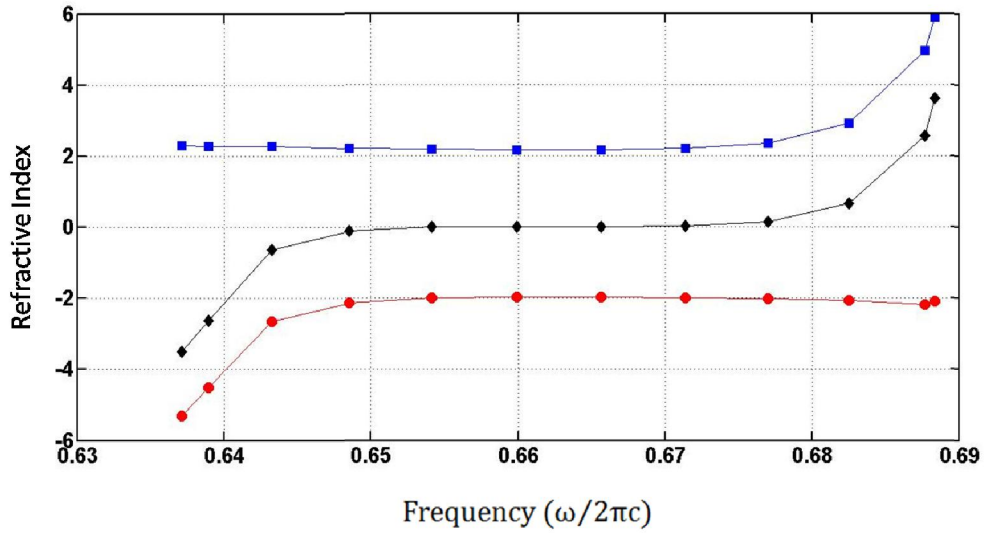
Figure 4.24 - Refractive index profile in regular PhC (blue),disordered PhC (red) and superlattice (black).

One of the plausible designing for these type of superlattices is the number of holes in each layer which determine the average zero index. In our suggested structure we choose the degree of disordered in a way to form integer number of holes for each side. We will study this to see the effect of variation of both thickness and number of stacks for some conceptual cases in this field later and see the advantages of having this priority over last case.
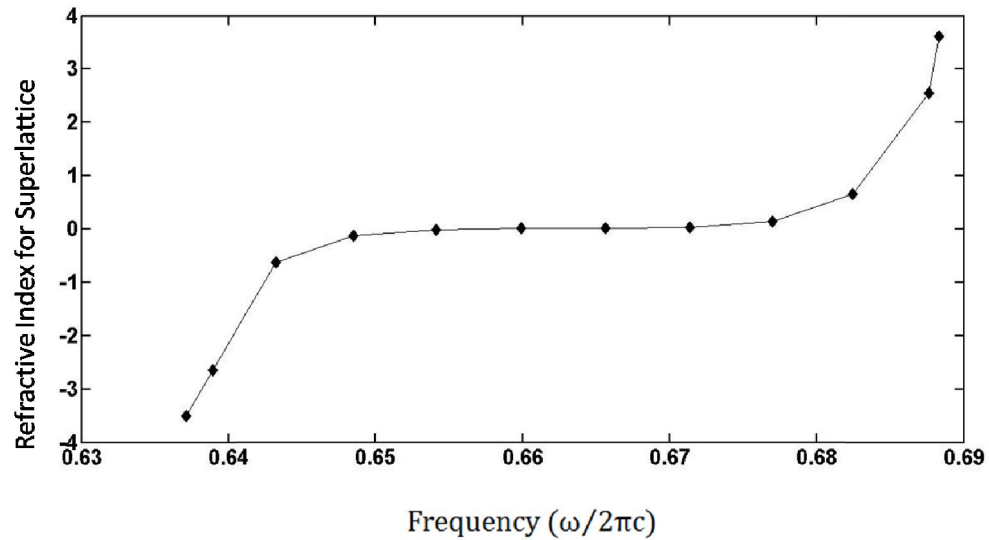
Figure 4.25 - Zoomedsection of symmetric refractive index profile in crystal-crystal superlattice vs. angular frequency.

## 4.4 Zero-ñ gap in Crystal-Crystal superlattice type

Combination of two types of crystals in atomic level ends up with huge number of achievements in electronic [83]. By reviewing all governing rules at atomic level, the matter of compatibility, energy states and feasibility of suggested materials are one of the challenging in this field. In solid-state devices, the matter of having either heterogeneous or homogeneous component is occupied in high level of consideration since play a major role at the desired results [84]. We also introduce the new type of PhCs in a homogeneous superlattice to gain zero-$\hat{n}$gap with an enhanced electric fieldand flux at the output of the suggested component. One of the advantages of having crystal-crystal superlattice instead of crystal-slab one is forming a zero-$\hat{n}$ gap with a symmetric transmission spectrum since the refractive-index profile of these suggested homogeneous structures approve the idea (Figure 4.25). Unlike the homogeneous structure having inhomogeneoussuperlattice, crystal-slab, gives rise to either short-band (Figure 3.12) zero index or two zero index at two separated range of frequencies

77

(Figure 3.13). Recently, so many attempts has been suggested to make negative refractive index materials , zero-$\tilde{n}$gap PhCs and complete photonic band gap to have an expected manipulation of light inside the matter. However, controlling phase of single mode in on-chip application relies on having symmetric refractive index profile, possessing positive, negative and zero index in broad range of frequencies, in short range of distance. This novel component toward the forming a component with symmetric refractive index profile in a broad band is a straightforward approach to fulfill all optical goals with the ease of designing step. In other words, there are so many alternative PhCs with the same parameters with many existed options. In this thesis, we suggest two modulated PhCs, one with the regular hexagonal structure and the other with disordered 34 degree to create a superlattice and make sure about combination of left hand side materials (LHM) with right hand side material to end up with the zero[th] order of gap.

As in on-chip devices the range of frequencies are limited having one constant dielectric like slab gives rise to limited parameters of PhC. In other words, to have zero-$\tilde{n}$gap at the range of 1500 [nm] ~1600 [nm] the parameters of PhCshould be arranged in a way to gain negative refractive index at this small range of frequencies. Even if one could find this which is a typical step the harder step is limited components of LHM since the number of holes have to be integer. One of the hardships of designing a structure with a computed ratio of ($d_1/d_2$) is limitation of cutting PhCs from the calculated thickness of either $d_1$ or $d_2$ to make a desired superlattice. In other words, it is not possible in reality to select a desired distance for LHM or RHM since the cutting line should end up at the symmetric potential values according to the periodicity of PhC. Thus, this calculated cutting lines should be designed in a way either to chose this crossing line exactly after a defined unit cell. However, all ($d_1/d_2$) ratios are not feasible except having alternative options of creating either right or left hand side materials with different segment size. Angle variation of hexagonal structure obviate this hardship step of computing and make ease of designing with variety of components in any desired wavelength since the

designer can chose any optional disordered angles. In this thesis, we combined 34 degree disordered hexagonal with the regular one to have superlattice of obtaining zero-$\hat{n}$gap. (Figure 4.26) illustrates the transmission spectrum of superlattice with respect to the number of holes in each section of superlattice and transmission spectrum of superlattice which forms the zero-$\hat{n}$gap at frequency of 0.657 with different number of holes. The parameters that we used to gain this zero phase delay, are as following: 0.32 [um] silicon on top of 1 [um] silicon dioxide with a hexagonal cylindrical holes (air) radii 0.35 and lattice constants are 0.5 [um] and 0.447 [um] for 30 and 34 degree respectively and also the ratio of $(d_1/d_2)$ is equal to $(ax_2 / ax_1)$ which $ax_2$ and $ax_1$ are shown in (Figure 4.4) of 30 and 34 degree respectively.
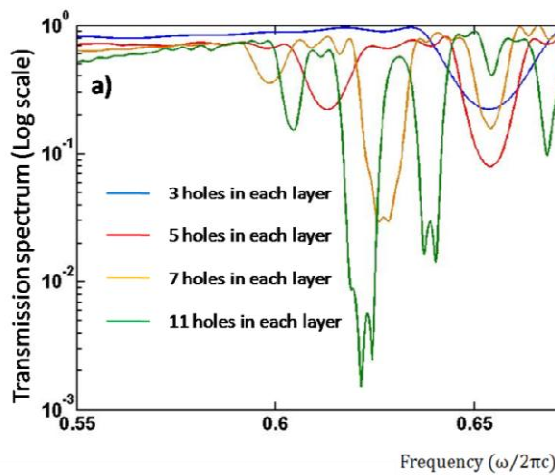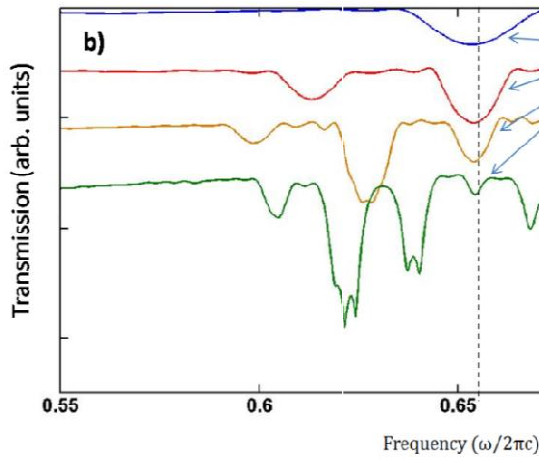
Figure 4.26 - Logarithmic normalized transmission spectrum plotin3, 5, 7 and 11 holes cases, a) Transmission spectrum in log scale, b) the existence of zero-ñ gap gives rise to no shifting in phase.

To compare two class of structure, homogeneous and inhomogeneous, we attached both results in zoomed in form to have better discussion on them in (Figure 4.27) and (Figure 4.28)
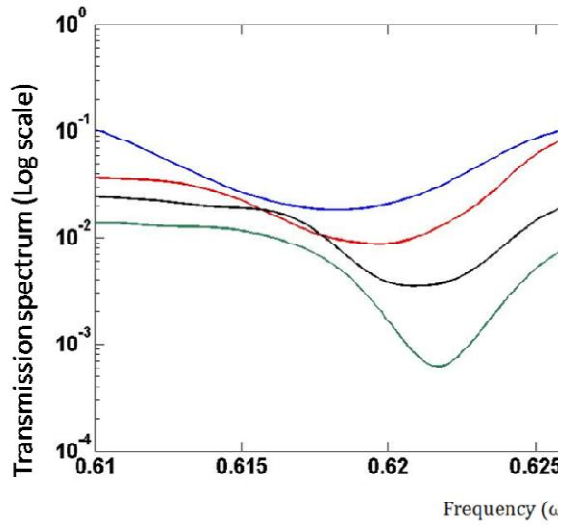
Figure 4.27 - Zoomed section of transmission spectrum for inhomogeneous (crystal-slab) superlattice that shows 1 decade of attenuation.

As it is clear from (Figure 4.27) the transmission spectrum suffer from attenuated signal and obviously there is no symmetric in the zero-ñ band section that is based on having unsymmetrical profile of refractive index which is presented in (Figure 3.12). Meaning that, the effective refractive index of suggested inhomogeneous structure have two negative refractive index in both sides of the zero index that leads to having unsymmetrical index profile. Unlike the inhomogeneous one, the effective refractive index profile in crystal-crystal structure (homogeneous) has symmetrical values including both negative and positive in both sides of the zero index (Figure 4.25).

81
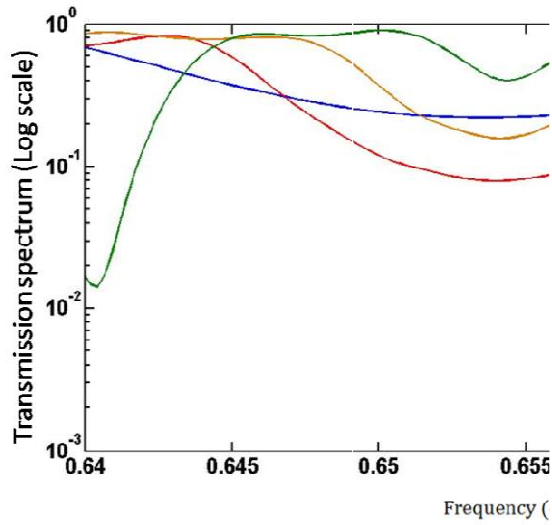
Figure 4.28 - Zoomed section of transmission spectrum for homogeneous (crystal-crystal) superlattice, (blue) 3holes, (red) 5 holes, (yellow) 7 holes and (green) 11 holes in each layer

In addition, we attached the larger structures to have acceptable contrast between transmission region and zero-ñ gap range of frequencies in (Figure 4.29).
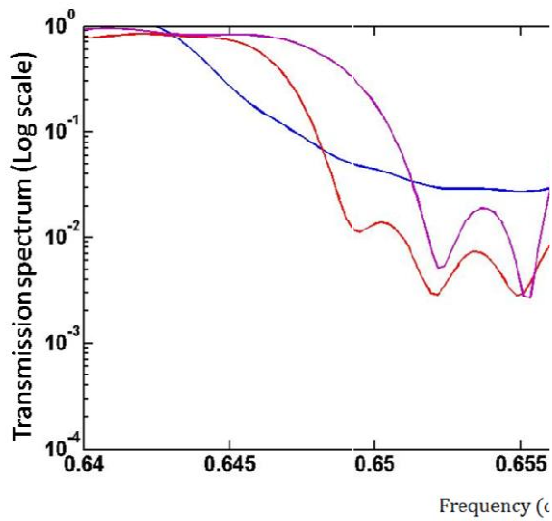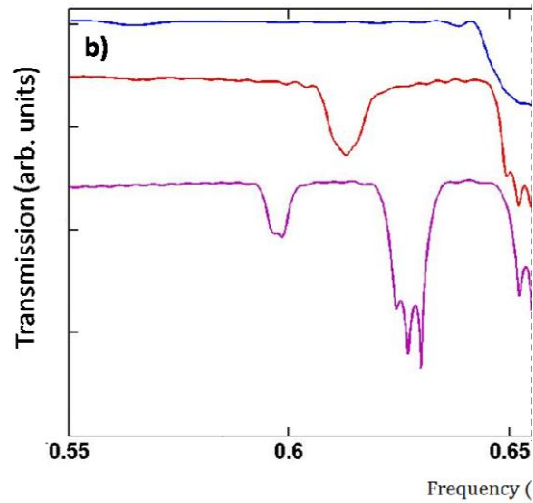
Figure 4.29 - Transmission spectrum for longer structure (8 stacks), a) zoomed zero-ñ gap with deep reflection spectra , b) existence of zero-ñ gap gives rise to no shift in phase

By considering the fact that, speed of light wave is constant in non-dispersive media, the Gaussian pulse function that contain multiple frequencies tend to have dispersion and lose the shape of pulse if the speed of applied light depends on frequency of the wave. Meaning that, higher frequencies tend to travel faster than lower frequencies and gives rise to pulse spread out and lose its shape as it travels. Not that the middle of the pulse is expected to travel with the same speed as already did but the only thing that fix this asymmetric dispersion is to have an asymmetric refractive index profile. In other words, providing a media with a zero index for the middle of the pulse and negative refractive index for higher frequency and positive values of index for the lower frequencies of the pulse give a chance of having the same speed through the lattice while it is travelling. As a result, we changed the properties of material by engineering it in a proper way to modify a dispersive media to a non-dispersive media. The results clarifies in (Figure 4.28) the non-dispersive profile of modulated structure.

Showing electric field distribution helps to have different perspective of what we achieved. In (Figure 4.30) we applied a continuous wave instead of Gaussian pulse to

monitor its flux at the end of the structure. This result shows the brag condition for all other frequencies except $\frac{1}{\lambda} = 0.655$ which included in the zero-$\hat{n}$ . In other words, applied planer wave comes out at the end with high transmission spectrum which is shown with the red-blue color.
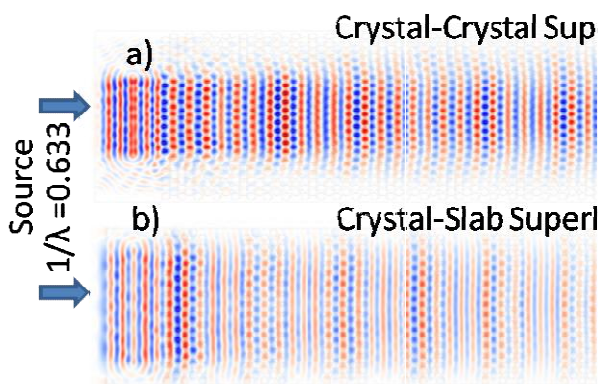


Figure 4.30 - The electric field (introduced from source with $^1/_{\lambda} = 0.633$) distribution through: a) crystal-crystal superlattice (5 holes 9 stacks) with the frequency from transmission range, b)crystal-slab superlattice (5 holes 10 stacks) with the frequency from transmission range experience destructive interaction between transmitting and reflecting light flow.

To compare this achieved result with the conventional one which are introducing slab for the positive layer, the attenuated electric field distribution is well clear that the structure does not let the wave flows with high transmission spectra due to constructive interference of going and coming wave inside the superlattice that is shown in (Figure 4.30b). On the other hand the obviated mentioned issue in suggested superlattice gives rise to no destructive Fresnel reflection and monitoring high transmission at the end of the developed component (Figure 4.30a). In addition, we attached the results of same layers (5 holes in each layer) to have clear comparison of two structures in (Figure 4.31) that shows increasing the number of stacks causes to lose transmission

84

more and more. However, increasing the length and number of stacks in (Figure 4.31a) shows no decaying in transmission at the end of the structure. As a result, this type of superlattices have no contrast while they have large geometry.
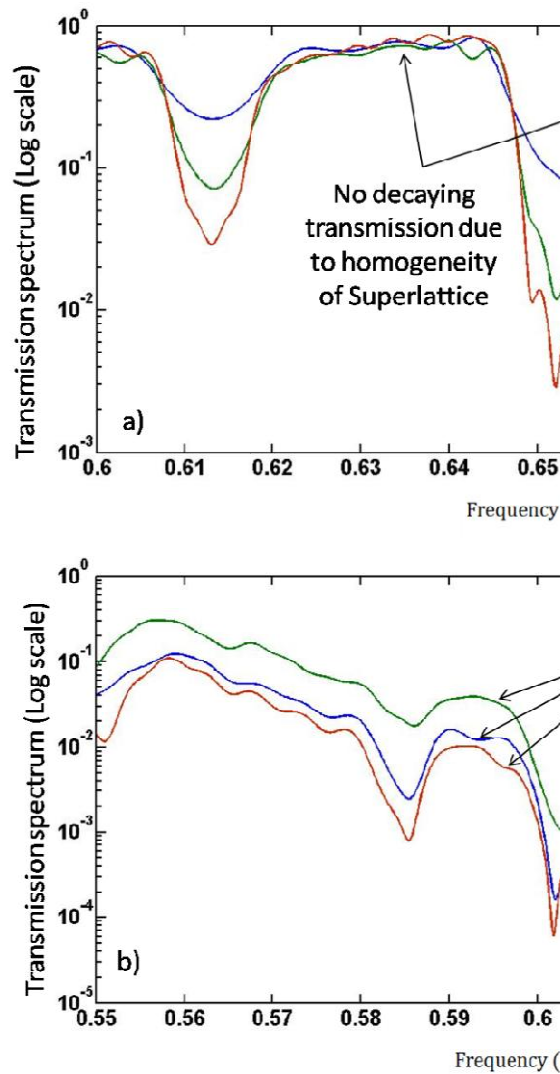


Figure 4.31 - Comparing transmission spectra in three different structures with the same thickness, a) homogeneous superlattice (crystal-crystal) with no decaying b) inhomogeneous superlattice (crystal-slab) cases decays with increasing the number of stacks.

As a conclusion, controlling phase and amplitude of light is only possible while we have an accurate values of band diagram which is obtained by solving Eigenvaluess. We

proceed this computational process using MPB and the whole results are in total agreement with each other. However, the preference of suggested modulation can be discussed through the comparison of (Figure 4.27) and (Figure 4.28) in which they are showing transmission spectra of both superlattices one with slab and the other applied disordered PhC. One simply recognizes that in the case of slab, whole transmission spectrum is one decade below from what we obtained in suggested modulation one. Meaning that the amount of applied light at the beginning of superlattice experience Fresnel reflection [74] due to facing with inhomogeneous structure and gives rise to destructive interference of light through the lattice. On the other hand, the modulated disordered structure improved this problem to gain high transmission spectrum with zero-ñ phase at the desired range of frequency.

## 4.5 Summary in future work

In this chapter, we learned the calculated band diagram of disordered structure that is a typical issue of fabrication. However, it has a logical road map of exploring and realizing these class of structures. In addition, it provides vast options of expected results and solutions to have an understanding of facing any error in research process. Moreover, we designed and used the modulation of hexagonal structure to form a crystal-crystal superlattice. In addition, by considering the theory behind what researchers are interested to scrutinize and get the step of action for any faced problems in their field of study, therefore, this knowledge would be a useful one. For example, we proved manipulation of photonic band gap without any modification in parameters involved with the regular hexagonal structure. Meaning that homogeneous fashion through lattice gives rise to have ease of manipulation based on controlling light flow. This approach provides swinging PBG which is one of the essential concerns of PhC science. This case of study also provides the predicted results and range of errors while we are dealing with imperfect tools of micro fabrication. In addition, we demonstrated existence of negative refractive index merely by variation of angles inside the suggested hexagonal structure. This ease of controlling in dispersion phenomena leads to design a

superlattice with a homogeneous structure and compare it with inhomogeneous one and some other experimental results. More importantly, this modulated homogeneous superlattice reduce Fresnell reflection since both sides of alternative stacks are PhC. In other words, this class of superlattice gives high transmission spectrum and consequently high sensitive signals for sensor applications. We also compute the refractive index profiles with a highly values in both negative and positive. It provides a great opportunity for one who needs to design a strong coupling of light with the component since the regular component does not possess vast options of alternating in particular rang of frequency. We will examine the defect-less waveguide merely by introducing the disorder instead of having defect path through the lattice. In addition, our next step is examining the experimental results of suggested modulated structure and go further and track the light's behavior in amorphous distribution of dielectric inside a particular lattice.

# REFERENCES

[1]. Almeida, Vilson R., et al. "All-optical control of light on a silicon chip." Nature 431.7012 (2004): 1081-1084.

[2]. Venkataraman, Vivek, KasturiSaha, and Alexander L. Gaeta. "Phase modulation at the few-photon level for weak-nonlinearity-based quantum computing." *Nature Photonics* 7.2 (2013): 138-141.

[3]. Hennessy, Kevin, et al. "Quantum nature of a strongly coupled single quantum dot–cavity system." Nature 445.7130 (2007): 896-899.

[4]. Kim, Hyochul, et al. "A quantum logic gate between a solid-state quantum bit and a photon." Nature Photonics 7.5 (2013): 373-377.

[5]. Bose, Ranojoy, et al. "All-optical coherent control of vacuum Rabi oscillations." Nature Photonics 8.11 (2014): 858-864.

[6]. Ren, M., et al. "An opto-mechanical coupled-ring reflector driven by optical force for lasing wavelength control." Applied Physics Letters 108.8 (2016): 081106.

[7]. Kaneko, Toshimitsu, Masaaki Okamoto, and Katsumi Uesaka. "Phase noise study of laser diodes with external optical feedback for digital coherent communications." Semiconductor Laser Conference (ISLC), 2016 International. IEEE, 2016.

[8]. Petta, Jason R., et al. "Coherent manipulation of coupled electron spins in semiconductor quantum dots." *Science* 309.5744 (2005): 2180-2184.

[9]. Yoon, Ki-Hong, et al. "2.5-Gb/s hybridly-integrated tunable external cavity laser using a superluminescent diode and a polymer Bragg reflector." Optics express 18.6 (2010): 5556-5561.

[10] . B. Liu, A. Shakouri, and J. E. Bowers, "Wide tunable double ring resonator coupled lasers," Appl. Phys. Lett. 79, 3561–3563 (2001).

[11]. Matsuo and T. Segawa, "Mircoring-resonator-based widely tunable lasers," IEEE J. Sel. Top. Quantum Electron. 15, 545–554 (2009)

[12]. M. C. Y. Huang, Y. Zhou, and C. J. Chang-Hasnain, "A Nanoelectromechanical tunable laser," Nat. Photonics 2, 180–184 (2008).

[13]. X. M. Zhang, A. Q. Liu, D. Y. Tang, and C. Lu, "Discrete wavelength tunable laser using microelectromechanical systems technology," Appl. Phys. Lett. 84(3), 329–331 (2004)

[14]. A. Q. Liu and X. M. Zhang, "A review of MEMS external-cavity tunable lasers," J. Micromech. Microeng. 17, R1–R13 (2007)

[15]. 9 H. Cai, A. Q. Liu, and X. M. Zhang, "A miniature tunable coupled-cavity laser constructed by micromachining technology," Appl. Phys. Lett. 92, 031105 (2008).

[16]. Lapine, M., Shadrivov, I.V., Powell, D.A. &Kivshar, Y.S. Magnetoelastic metamaterials. Nature Mater. 11, 30–33 (2012).

[17]. Zhang, J., MacDonald, K.F. &Zheludev, N.I. Nonlinear dielectric optomechanical metamaterials. Light Sci. Appl. 2, e96 (2013).

[18]. Zhao, R., Tassin, P., Koschny, T. &Soukoulis, C.M. Optical forces in Nanowire pairs and metamaterials. Opt. Express 18, 25665–25676 (2010).

[19]. Karvounis, A., Ou, J.Y., Wu, W., MacDonald, K.F. &Zheludev, N.I. Nano-optomechanical nonlinear dielectric metamaterials. Appl. Phys. Lett. 107, 191110 (2015).

[20]. M. L. Povinelli, M. Lončˇar, and J. D. Joannopoulos, "Evanescent-wave bonding between optical waveguide," Opt. Lett. 30, 3042–3044 (2005).

[21]. M. Li, W. H. P. Pernice, C. Xiong, T. Baehr-Jones, M. Hochberg, and H. X. Tang, "Harnessing optical force in integrated photonics circuits," Nature 456, 480–485 (2008).

[22]. Y. F. Yu, M. Ren, J. B. Zhang, T. Bourouina, C. S. Tan, J. M. Tsai, and A. Q. Liu, "Force-induced optical nonlinearity and Kerr-like coefficient in opto-mechanical ring resonators," Opt. Express 20, 18005–18015 (2012)

[23]. 5B. Dong, H. Cai, G. I. Ng, P. Kropelnicki, J. M. Tsai, A. B. Randles, M. Tang, Y. D. Gu, Z. G. Suo, and A. Q. Liu, "A Nanoelectromechanical systems actuator driven and controlled by Q-factor attenuation of ring resonator," Appl. Phys. Lett. 103, 181105 (2013).

[24]. M. Ren, J. Huang, H. Cai, J. M. Tsai, J. Zhou, Z. Liu, Z. Suo, and A. Q. Liu, "Nano-opto-mechanical actuator and "pull-back" instability," ACS Nano 7, 1676–1681 (2013).

[25]. 3H. Tian and J. Zi, Opt. Commun. 252, 321 (2005)

[26]. Debord, R. Jamier, F. Gerome, O. Leroy, C. Boisse-Laporte, P. Leprince, L. L. Alves, and F. Benabid, Opt. Express 21, 25509 (2013).

[27]. F. Couny, F. Benabid, P. J. Roberts, P. S. Light, and M. G. Raymer, Science 318, 1118 (2007).

[28]. A. Ermolov, K. F. Mak, M. H. Frosz, J. C. Travers, and P. St.J. Russell, Phys. Rev. A 92, 033821 (2015).

[29]. . O. H. Heckl, C. R. E. Baer, C. Kränkel, S. V. Marchese, F. Schapper, M. Holler, T. Südmeyer, J. S. Robinson, J. W. G. Tisch, F. Couny, P. Light, F. Benabid, and U. Keller, Appl. Phys. B 97, 369 (2009).

[30]. Yao, Wen-Gang, et al. "Mode-Selecting Micrograting Cavity Laser." Journal of Lightwave Technology 34.17 (2016): 4143-4147.

[31]. B. E. Little, J. S. Foresi, G. Steinmeyer, E. R. Thoen, S. T. Chu, H. A. Haus,E. P. Ippen, L. C. Kimerling, and W. Greene, "Ultra-compact SiSiO2 microring resonator optical channel dropping filters," IEEE Photonic. Tech. L., vol. 10, no. 4, pp. 549-551, Apr. 1998.

[32]. F. Vollmer and S. Arnold, "Whispering-gallery-mode biosensing: label-free detection down to single molecules," Nat. Methods, vol. 5, no. 7, pp. 591-596, Jul. 2008.

[33]. J. Su, A. F. G. Goldberg, B. M. Stoltz, "Label-free detection of single Nanoparticles and biological molecules using microtoroid optical resonators," Light: Sci. Appl., vol. 5, no. e16001, Jan. 2016.

[34]. C. Xiang, W. Koo, F. So, H. Sasabe, and J. Kido, "A systematic study on efficiency enhancements in phosphorescent green, red and blue microcavity organic light emitting devices," Light: Sci. Appl., vol. 2, no. e74, Jun. 2013.

[35]. A. J. Shields, "Semiconductor quantum light sources," Nature Photon., vol. 1, no. 4, pp. 215-223, Apr. 2007.

[36]. J. M. Gérard, B. Sermage, B. Gayral, B. Legrand, E. Costard, and V. Thierry-Mieg, "Enhanced spontaneous emission by quantum boxes in a monolithic optical microcavity," Phys. Rev. Lett., vol. 81, no. 5, Aug. 1998.

[37]. C. Zhang, C. L. Zou, Y. L. Yan, C. Wei, J. M. Cui, F. W. Sun, J. Yao, and Y. S. Zhao, "Self-Assembled Organic Crystalline Microrings as Active Whispering-Gallery-Mode Optical Resonators," Adv. Opt. Mater., vol. 1, no. 5, pp. 357-361, May. 2013

[38]. ]X. Wang, Q. Liao, Q. Kong, Y. Zhang, Z. Xu, X. Lu, and H. Fu, "Whispering-Gallery-Mode Microlaser Based on Self-Assembled Organic Single-Crystalline Hexagonal Microdisks," Angew. Chem.- Int. Edit., vol. 53, pp. 5863-5867, Jun 2014.

[39]. J. Li, S. Zhang, R. Yu, D. Zhang, and Y. Wu, "Enhanced optical nonlinearity and fiber-optical frequency comb controlled by a single atom in a whispering-gallery-mode microtoroid resonator," Phys. Rev. A., vol. 90, no. 5, p. 053832, Nov. 2014.

[40]. S. Kalusniak, S. Sadofev, S. Halm and F. Henneberger, "Vertical cavity surface emitting laser action of an all monolithic ZnO-based microcavity," Appl. Phys. Lett., vol. 98, no. 1, p. 011101, Jan. 2011.

[41]. Chen, E. Towe, "Nanowire lasers with distributed-Bragg-reflector mirrors," Appl. Phys. Lett., vol. 89, no. 5, p. 053125. Aug. 2006.

[42]. Vahala, Kerry J. "Optical microcavities." Nature 424.6950 (2003): 839-846.

[43]. Sun-Goo Lee, Jin-sun Choi, Jae-Eun Kim, Hae Yong Park, and Chul-SikKee, "Reflection minimization at two-dimensional photonic crystal interfaces," Opt. Express 16, 4270-4277 (2008)

[44]. J. Witzens, M. Loncar, and A. Scherer, "Self-collimation in planar photonic crystals," IEEE J. Sel. Top. Quantum Electron. 8, 1246–1257 (2002).

[45]. S. Foteinopoulou, E. N. Economou, and C. M. Soukoulis, "Refraction in media with a negative refractive index," Phys. Rev. Lett. 90, 107402 (2003).

[46]. R. A. Shelby, D. R. Smith, and S. Schultz, "Experimental verification of a negative index of refraction," Science 292, 77-79 (2001).

[47]. Arlandis, Julien, et al. "From zero-average index metamaterials to zero-dispersion curvature photonic crystal superlattices for self-collimation of light." SPIE Photonics Europe. International Society for Optics and Photonics, 2012.

[48]. D. W. Prather, S. Shi, D. M. Pustai, C. Chen, S. Venkataraman, A. Sharkawy, G. J. Schneider, and J. Murakowski, "Dispersion-based optical routing in photonic crystals," Opt. Lett. 29, 50-52 (2004).

[49]. P. T. Rakich, M. S. Dahlem, S. Tandon, M. Ibanescu, M. Soljačiˇ´v, G. S. Petrich, J. D. Joannopoulos, L. A. Kolodziejski, and ErichP. Ippen, "Achieving centimetre-scale supercollimation in a large-area two-dimensional photonic crystal," Nat. Mater. 5, 93–96 (2006).

[50]. X. Yu and S. Fan, "Bends and splitters for self-collimated beams in photonic crystals," Appl. Phys. Lett. 83, 3251–3253 (2003).

[51]. Z. Y. Li and L. L. Lin, "Evaluation of lensing in photonic crystal slabs exhibiting negative refraction," Phys. Rev. B 68, 245110 (2003).

[52]. J. D. Joannopoulos, R. D. Meade, and J. N. Winn, "Photonic Crystals: Molding the Flow of Light," Princeton University Press, New Jersey, 1995.

[53]. BabakMomeni, Majid Badieirostami, and Ali Adibi, "Accurate and efficient techniques for the analysis of reflection at the interfaces of three-dimensional photonic crystals," J. Opt. Soc. Am. B 24, 2957-2963 (2007)

[54]. Goi, Elena, et al. "Complete bandgap in three-dimensional chiral gyroid photonic crystals for topological photonics." CLEO: Science and Innovations. Optical Society of America, 2016.

[55]. Peng, Siying, et al. "Three-dimensional single gyroid photonic crystals with a mid-infrared bandgap." ACS Photonics (2016).

[56]. Ishizaki, Kenji, et al. "Realization of three-dimensional guiding of photons in photonic crystals." Nature Photonics 7.2 (2013): 133-137.

[57]. S. G. Romanov, P. Ferrand, M. Egen, R. Zentel, J. Ahopelto, N. Goponik, A. Eychmüller, A. Rogach, and C. M. Sotomayor Torres, "Exploring integration prospects of opalbased photonic crystals," Synth. Met. 139, 701–704 (2003).

[58]. E. Istrate, A. A. Green, and E. H. Sargent, "Behavior of light at photonic crystal interfaces," Phys. Rev. B 71, 195122 (2005).

[59]. M. Deubel, M. Wegener, S. Linden, G. von Freymann, and S. John, "3D–2D–3D photonic crystal heterostructures fabricated by direct laser writing," Opt. Lett. 31, 805–807 (2006).

[60]. Fan, Shanhui. "Manipulating light with photonic crystals." Physica B: Condensed Matter 394.2 (2007): 221-228

[61]. Chigrin, Dmitry N. Electromagnetic waves propagation in photonic crystals with incomplete photonic bandgap. Diss. Universität Wuppertal, FakultätfürElektrotechnik, Informationstechnik und Medientechnik» Elektrotechnik» Dissertationen, 2004.

[62]. S. Zhang, W. Fan, K. J. Malloy, S. Brueck, N. C. Panoiu, and R. M. Osgood, Opt. Express 13, 4922 (2005).

[63]. J. Valentine, S. Zhang, T. Zentgraf, E. Ulin-Avila, D. A. Genov, G. Bartal, and X. Zhang, Nature (London) 455, 376 (2008).

[64]. John, Sajeev. "Strong localization of photons in certain disordered dielectric superlattices." Physical review letters 58.23 (1987): 2486.

[65]. García, Pedro David, and Peter Lodahl. "Light-matter interaction in disordered photonic Nanostructures." arXiv preprint arXiv:1611.02038 (2016).

[66]. Deng, Hanying, et al. "Tunability and Robustness of Dirac Points of Photonic Nanostructures." IEEE Journal of Selected Topics in Quantum Electronics 22.5 (2016): 1-9.

[67]. Savić-Šević, Svetlana, et al. "Localization of light in a polysaccharide-based complex Nanostructure." Optical and Quantum Electronics 48.5 (2016): 1-5.

[68]. Henini, Mohamed, ed. Handbook of self assembled semiconductor Nanostructures for novel devices in photonics and electronics. Elsevier, 2011.

[69]. Habib, MdSelim, et al. "Proposal for highly birefringent broadband dispersion compensating octagonal photonic crystal fiber." Optical Fiber Technology 19.5 (2013): 461-467.

[70]. Johnson, Steven G., and John D. Joannopoulos. "Block-iterative frequency-domain methods for Maxwell's equations in a planewave basis." Optics express 8.3 (2001): 173-190.

[71]. Jackson, John David. Classical electrodynamics. Wiley, 1999.

[72]. Slusher, Richart E., and Benjamin J. Eggleton, eds. Nonlinear photonic crystals. Vol. 10. Springer Science & Business Media, 2013.

[73]. Kocaman, S., et al. "Observation of zeroth-order band gaps in negative-refraction photonic crystal superlattices at near-infrared frequencies." Physical review letters 102.20 (2009): 203905

[74]. Xi, J-Q., et al. "Optical thin-film materials with low refractive index for broadband elimination of Fresnel reflection." Nature photonics 1.3 (2007): 176-179.

[75]. Satheesh, D. J., and JayakumariIsac. "Optical Analysis, Urbach and Bandgap Energy of Mn0. 8 Zn0. 2TixFe2-2xO4 with x= 0.15-Manganese-Zinc Ferrite system doped with Titanium."

[76]. Pollock, Clifford R., and Michal Lipson. Integrated photonics. Vol. 20. No. 25. 2003.]

[77]. Kocaman, S., et al. "Observation of zeroth-order band gaps in negative-refraction photonic crystal superlattices at near-infrared frequencies." Physical review letters 102.20 (2009): 203905.

[78]. Chatterjee, Rohit, et al. "Achieving subdiffraction imaging through bound surface states in negative refraction photonic crystals in the near-infrared range." *Physical review letters* 100.18 (2008): 187401.

[79]. Chatterjee, Rohit, et al. "Achieving subdiffraction imaging through bound surface states in negative refraction photonic crystals in the near-infrared range." Physical review letters 100.18 (2008): 187401.

[80]. Kocaman, S., et al. "Zero phase delay in negative-refractive-index photonic crystal superlattices." Nature Photonics 5.8 (2011): 499-505

[81]. Li, Yang, et al. "On-chip zero-index metamaterials." Nature Photonics 9.11 (2015): 738-742.

[82]. Kocaman, Serdar, et al. "Controlled zero-ñ bandgaps in negative refraction photonic superlattices for wavefront control and open resonances." Conference on Lasers and Electro-Optics. Optical Society of America, 2009.

[83]. Koechner, Walter. Solid-state laser engineering. Vol. 1. Springer, 2013.

[84]. Wang, Hongyue, et al. "Transport in a Single Self-Doped Nanocrystal." ACS Nano (2017).